Nuclear Engineering and Design 63 (1981) 199–231
North-Holland Publishing Company

STARFIRE, A COMMERCIAL TOKAMAK POWER PLANT DESIGN

C.C. BAKER, M.A. ABDOU, C.D. BOLEY, A.E. BOLON *, J.N. BROOKS, R.G. CLEMMER, D.A. EHST, K. EVANS, Jr., P.A. FINN, R.E. FUJA, Y. GOHAR, J. JUNG, W.J. KANN, R.F. MATTAS, B. MISRA, H.L. SCHREYER, D.L. SMITH, H.C. STEVENS and L.R. TURNER
Argonne National Laboratory, Argonne, IL 60439, USA

D.A. DE FREECE, C. DILLOW, G.D. MORGAN and C.A. TRACHSEL
McDonnell Douglas Astronautics Company, P.O. Box 516, St. Louis, MO 63166, USA

D. GRAUMANN, J. ALCORN, R.E. FIELDS and R. PRATER
General Atomic Company, P.O. Box 81608, San Diego, CA 92138, USA

J. KOKOSZENSKI, K. BARRY, M. CHERRY and H. KLUMPE
The Ralph M. Parsons Company, 100 West Walnut Street, Pasadena, CA 91124, USA

R.W. CONN **, G.A. EMMERT, I.N. SVIATOSLAVSKY and D.K. SZE
Nuclear Engineering Department, University of Wisconsin, Madison, WI 53706, USA

Received 9 October 1980

STARFIRE is a design for a conceptual commercial tokamak electrical power plant based on the deuterium/tritium/lithium fuel cycle. In addition to the goal of being technologically credible, the design incorporates safety and environmental considerations. STARFIRE is considered to be the tenth in a series of commercial fusion power plants.

STARFIRE has a 7-m major radius reactor producing 1200 MW of net electrical power from 4000 MW of thermal power, with an average neutron wall load of 3.6 MW/m^2. The aspect ratio is 3.6 and a D-shaped plasma with a height-to-width ratio of 1.6 and average toroidal beta of 0.067 is used. The maximum magnetic field is 11T. Availability goals have been set at 85% for the reactor and 75% for the complete plant including the reactor.

The major features for STARFIRE include a steady-state operating mode based on a continuous rf lower-hybrid current drive and auxiliary heating, solid tritium breeder material, pressurized water cooling, limiter/vacuum for impurity control, most superconducting EF coils outside the TF superconducting coils, fully remote maintenance, and a low-activation shield.

1. Introduction

The objective of the STARFIRE study is to develop a design concept for a commercial tokamak electric power plant based on the deuterium/tritium/lithium-fuel cycle. The key technical objective is to develop an attractive embodiment of the tokamak as a power reactor consistent with credible engineering solutions to design problems. Another goal of the study is to give careful attention to the safety and environmental features of a commercial fusion reactor. This paper describes the major features of the reference reactor concept. A detailed report, including a description of the entire plant and a cost estimate, will be issued in October 1980.

The basic guidelines for STARFIRE assume the

* On leave from The University of Missouri-Rolla, Rolla, MO 65401, USA.
** Present address: School of Engineering and Applied Sciences, University of California, Los Angeles, CA 90024, USA.

successful operation of a tokamak engineering test facility (ETF) and a demonstration power plant. STARFIRE is considered to be the tenth plant in a series of commercial reactors. It is, therefore, assumed that a well-established vendor industry exists and that utilities have gained experience with the operation of fusion plants.

A major feature for STARFIRE is a steady-state operating mode based on a continuous plasma current drive. An rf lower-hybrid current drive option has received the most attention in the study. The potential advantages of steady-state reactor operation are numerous and are discussed in detail in the next section.

Availability goals have been established as 85% for the reactor and 75% for the complete plant including the reactor. These goals provide a basis for design of maintenance equipment. The maintenance scenario incorporates the current utility practice of shutting down annually for one month and a four month shutdown approximately every five to ten years.

An important design consideration is the choice of the plasma impurity and alpha-particle removal concept. Initial investigations indicate that modest pumping of helium with a limiter/pumping system (~25% of the alpha-particle flux) coupled with about a 1.5-T margin in the maximum toroidal field should eliminate the need for a divertor. This result is based on the provision that a significant portion of the alpha-particle heating power can be radiated to the first wall rather than be deposited on the limiter. In general, a non-divertor option is greatly preferred from an overall reactor engineering point of view.

Another key design consideration is the location of the equilibrium field (EF) coils. The basic design approach is to locate almost all the EF coils outside of the toroidal field (TF) coils. All such EF coils would be superconducting. A limited number of segmented copper coils are located inside the TF coils, but outside of the blanket and shield.

Safety has played a major role in considering various blanket options. Solid tritium breeders are being emphasized in this study. In addition, efforts are being made to minimize the tritium inventory in the plasma exhaust processing systems and the radioactivity induced in the materials in the magnets and shield.

Section 2 presents the rationale for key design choices and provides an overview of the STARFIRE reference design. Section 3 describes the highlights of the major reactor subsystems and the maintenance approach is discussed in section 4. Details of the STARFIRE study are given in ref. [1].

2. Overview of the reactor concept

This section presents an overview of the STARFIRE reference design. Section 2.1 reviews the key considerations in the design point selection and section 2.2 describes the major features of the reference design.

2.1. Design point selection

Extensive system and trade-off studies were performed to support the selection process for the major parameters and design features of the STARFIRE commercial reactor. A summary of key results is presented in this subsection.

2.1.1. Reactor power

A survey of anticipated utility requirements in the STARFIRE time frame indicated power units of 1000-1500 MWe are most desirable. The fusion power was selected as 3490 MW which results in 4000 MW thermal power and 1200 MW of net electrical output.

2.1.2. Plasma burn mode

Theory and experiments indicate the possibility that toroidal plasma currents may be maintained in tokamaks with noninductive external momentum sources to the electrons. This suggests that steady state may be an achievable mode of operation for tokamaks. Steady-state operation offers many technological and engineering benefits in commercial reactors. Among these are: (1) component and system reliability is increased; (2) material fatigue is eliminated as a serious concern; (3) higher neutron wall load is acceptable; (4) thermal energy storage is not required; (5) the need for an intermediate coolant loop is reduced; (6) electrical energy storage is significantly reduced or eliminated; and (7) an ohmic heating solenoid is not needed, and external placement of the EF coils is simplified. It has been estimated that the combined benefits of steady state can

result in a saving in the cost of energy as large as 30%.

The penalty for steady-state operation comes primarily from potential problems associated with a noninductive current driver; in particular: (1) the electrical power requirements; (2) the capital cost; and (3) reliability and engineering complexity of the current driver. In STARFIRE, a lower-hybrid (LH) rf system is utilized for the dual purpose of plasma auxiliary heating and current drive. The penalty associated with the LH current drive is ~12–15% of the nominal cost and power requirements. Therefore, the choice of steady state as the operating mode in STARFIRE results in a net saving in the cost of energy of ~15%. Much larger savings are potentially realizable if the performance of the LH current driver can be further improved or substantially better alternatives for the current driver are developed.

2.1.2 Reactor size

Two principal parameters that greatly influence the desirable reactor size are: (1) the maximum achievable fusion power density, P_p averaged over the plasma volume; and (2) the maximum allowable neutron wall load, P_{nw}. The fusion power density, P_p, varies as $\beta_t^2 B_t^4$, where β_t is the ratio of the plasma to the magnetic pressure and B_t is the toroidal field at the plasma geometrical center. The plasma β_t is limited by stability considerations and is taken in this work as $0.24/A$, where A is the aspect ratio. The maximum magnetic field is limited by technology constraints. The niobium–titanium superconductor is practically limited to a maximum field of ~10 T while Nb_3Sn is capable of generating higher fields. Although present experience with Nb_3Sn is limited, the progress in the current technology development program justifies the assumption that the Nb_3Sn technology will be available in the STARFIRE time frame. It should be noted, however, that accommodating the electromagnetic forces associated with high fields adds significantly to the reactor engineering complexity.

The fusion power density in the plasma, P_p, and the neutron wall load, P_{nw}, cannot be selected independently as they are correlated by the following relationship:

$$P_f = P_{nw} A_w \left(\frac{17.6}{14.1}\right) = P_p V ,$$

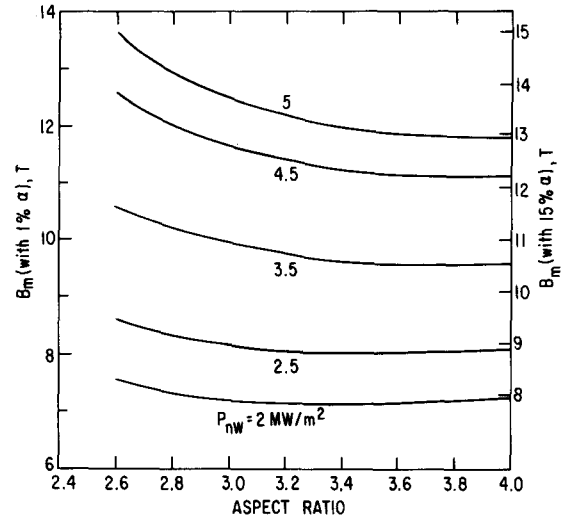

Fig. 1. B_m as a function of A at several values of P_{nw}. The LHS scale is for $n_\alpha/n_{DT} = 0.01$ and the RHS scale is for $n_\alpha/n_{DT} = 0.15$ (P_f = 3200 MW, $\beta_t = 0.24/A$, Δ_{BS}^i = 1.2 m, Δ_v = 0.1 m, T_e = 8 keV, κ = 1.6.)

where P_f is the reactor fusion power, A_w is the surface area of the first wall, and V is the plasma volume. Fig. 1 shows the maximum toroidal field B_m required as a function of aspect ratio, A, for P_f = 3200 MW, $\kappa = 1.6$, $\beta_t = 0.24/A$, scrape-off thickness, Δ_v = 0.1 m, and inner blanket/shield thickness, Δ_{BS}^i = 1.2 m. The scale on the left side shows the B_m required if a very efficient impurity control system is utilized such that the alpha-particle concentration, $n_\alpha/n_{DT} = 0.01$. The scale on the right shows the B_m required if a lower alpha-particle removal efficiency is assumed so that $n_\alpha/n_{DT} = 0.15$. As will be discussed later, accepting low alpha-particle removal efficiency permits the use of a simple limiter/vacuum system for plasma purity control and exhaust.

The maximum allowable neutron wall load is a function of the structural material, coolant, and design of the first wall. Limitations on the maximum structural temperature and thermal stress are often important constraints and these are sensitive to the surface heat load on the first wall. Steady-state plasma operation reduces fatigue as a constraint, thus permitting higher neutron wall load, higher thermal stress designs. On the other hand, radiating most of the alpha-particle heating power to the first wall increases the surface heat load and lowers the allow-

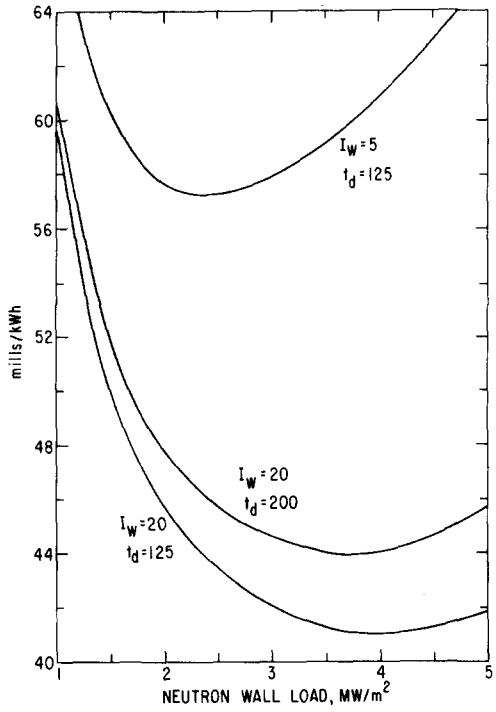

Fig. 2. Cost of energy as a function of neutron wall load. I_w is the integral neutron wall load in MW-yr/m^2 and t_d is the total downtime in days for replacement of the structural material. Results are based on fusion power of 3200 MW, aspect ratio of 3.6, plasma elongation of 1.6, and β_t = 0.067.

able neutron wall load. Other considerations that limit the neutron wall load are the coolant pumping power and the structure lifetime. Fig. 2 shows the cost of energy as a function of the neutron wall load at two values of the integral neutron wall load, I_w, of 5 and 20 MW-yr/m^2 and at two different values for the total cumulative downtime, t_d, for replacement of the structural material. For I_w = 5 MW-yr/m^2 and t_d = 125 d, the neutron wall load should be kept at ~2–2.5 MW/m^2. For I_w = 20 MW-yr/m^2 the cost of energy (COE) decreases significantly as the neutron wall load is increased from 1–2 MW/m^2. A smaller, but significant, saving in COE is realizable by increasing P_{nw} from 2–3 MW/m^2. A slight change in COE is noticeable in the range P_{nw} ~ 3–4 MW/m^2. These results assumed water coolant and modified austenitic steel structure in the first wall. Structural materials with better thermomechanical properties and radiation damage resistance can show a more pronounced saving in COE at higher neutron wall loads. The average neutron wall load in STARFIRE is selected as 3.6 MW/m^2 with an average surface heat load of ~0.9 MW/m^2. Poloidal variations in the surface heat load and neutron flux result in a peak-to-average ratio of ~1.2.

With the fusion power and neutron wall load selected, the surface area of the first wall is determined and the plasma elongation and aspect ratio are the only two parameters required to completely describe the plasma geometry. A D-shaped plasma with a height-to-width ratio (κ) of 1.6 was selected. This was found to be nearly the upper limit on elongation if the important design goal of locating most of the coils external to the TF coils is to be achieved. A detailed tradeoff analysis was performed to determine the optimum aspect ratio [2]. The most dominant effects tend to be the higher stability limit for β at lower aspect ratio and the reduced electrical power requirement for the H plasma current driver at larger aspect ratio. An aspect ratio of 3.6 yields the minimum COE. For the STARFIRE conditions, this results in a plasma major radius of 7 m and a half-width of 1.94 m.

2.1.4. Energy conversion

Solid lithium compounds are selected for the tritium breeder blanket in STARFIRE as they offer safety advantages compared to liquid lithium. The most attractive coolant candidates with solid tritium breeders are water and helium. A comparative study of the two coolants was performed. The study proved to be rather complex as there are approximately 15 technical areas of the reactor affected by the coolant choice. Nevertheless, the study showed clear advantages for the choice of water for the conditions of STARFIRE. Key points from the study are summarized below.

Helium cooling is an advanced technology with potentially higher conversion efficiency than pressurized water. However, a key problem that must be clearly recognized is that there is no structural material identified at present that can operate at high temperature, is compatible with helium, and has good resistance to radiation damage. Structural material temperatures <500°C are not capable of utilizing the full potential of helium. With modified austenitic stainless steel, the maximum coolant exit temperature

is 475°C with helium and 320°C with water. The obtainable thermodynamic efficiency depends on the steam temperature which in turn depends on the pinch-point temperature difference in the steam generator. To keep the cost of the steam generator reasonable, a pinch point of ~10°C is normally maintained with water and ~50–100°C with helium. The gross thermodynamic efficiency, η, is in the range of 36–39% for helium coolant and 34–36% for pressurized water.

Another major difference between the two coolants is the pumping power requirements. These are low with pressurized water, typically ~0.3% of the thermal power. The pumping power for helium is generally large and is approximately inversely proportional to the square of the helium pressure and coolant temperature rise. Helium coolant pressures much in excess of 1000 psi require extrapolation in technology. The magnitude of the coolant temperature rise is severely limited by the constraint on the maximum coolant exit temperature discussed above. It was estimated that the pumping power for helium at 1000 psi is $\geqslant$ 3% of the thermal power.

In STARFIRE, stipulation of a solid breeder blanket is an important feature. All useful solid breeders that satisfy the tritium recovery and material compatibility constraints require a neutron multiplier and have much lower tritium breeding potential than liquid lithium. The relatively large percentage of the structural material required with the helium coolant does not permit development of blanket designs with a reasonably conservative margin in the tritium breeding ratio. It was concluded from the neutronics analysis that a blanket breeding region must be placed on the inner side of the torus. This conclusion strongly impacts the helium/water comparison in view of the negative effect of void space in the inner blanket on tokamak reactor performance and economics. For a given plasma geometry, beta, and maximum toroidal field, the fusion power varies with the inner blanket/shield thickness, Δ^{i}_{BS}, as

$$P_f \sim \left(\frac{R - a - \Delta_v - \Delta^{i}_{BS}}{R}\right)^4,$$

where R is the major radius, a is the plasma half-width, and Δ_v is the scrape-off thickness. For STARFIRE, R = 7 m, a = 1.94 m, and Δ_v = 0.2 m. The required blanket/shield thickness with water coolant is Δ^{i}_{BS} = 1.2 m.

Helium requires $\Delta^{i}_{BS} = 1.2 + \delta$, where δ is the equivalent thickness of the void space for the helium coolant in the inner blanket. Solid breeder blanket module designs were developed in sufficient detail to permit reasonable estimates of δ. Typically, for 1000 psi helium, δ was found to be ~0.38 m with 0.18 m void in the blanket region and 0.2 m equivalent void space for manifolds and headers. The void space can be reduced by increasing the helium pressure. Furthermore, clever routing of the coolant manifolds and locating the headers further away from the midplane will substantially reduce δ, but will also significantly increase the coolant pumping power requirements.

Table 1
Summary of key points in the water and helium coolants comparison for STARFIRE
(Reference parameters: R = 7 m, a = 1.94 m, Δ_v = 0.2 m, B_m = 11.1 T, β_t = 0.067)

	Water	Helium
Pressure (psi)	2200	1000
Δ^{i}_{BS} (m)	1.20	1.38
B_0 (T)	5.80	5.52
Thermal power (MW)	4000	3273
Coolant exit temperature (°C)	320	475
Gross thermal efficiency (%)	36	39
Gross electric power (MW)	1440	1305
Coolant pumping power (MW)	15	95
rf electric power (MW)	150	150
Other auxiliary power (MW)	75	75
Net electric power (MW)	1200	985
Cost of primary coolant loop (M$)	45	102
$/kWe (relative)	1.0	1.26

Table 1 shows a comparison of STARFIRE performance with water and helium coolants. The void space thickness with helium cooling is taken as 0.18 m and has a substantial impact on the results of the comparison. For the conditions considered here, the net electrical power output is 1200 and 985 MW with pressurized water and helium, respectively. The cost of the primary coolant loops (pipes, pumps, and steam generators) is much more expensive with helium than with water. The net effect is that the cost per unit power is ~26% higher with helium than with water for the typical conditions in STARFIRE.

Several other areas of comparison between the two coolants were considered but they were found to be less important than the areas discussed above.

2.2. Reactor description

The reactor cross section is shown in fig. 3 and the major parameters are listed in table 2. The major reactor features are shown in the isometric drawing of fig. 4. All superconducting EF coils are located outside the twelve TF coils and four small segmented copper coils are located inside for plasma stability control. The shield provides the primary vacuum boundary. Twelve shield access doors are provided to permit removal of twenty-four toroidal blanket sectors. The cooling lines and rf ducts protrude through the shield doors so that high-pressure coolant disconnects can be located outside the vacuum boundary where small leaks could be tolerated.

Plasma startup is accomplished by electrically breaking down the deuterium-tritium gas using a ~3-MW electron cyclotron resonant heating (ECRH) system, inducing 1 MA of plasma current with OH coils and building up and sustaining the 10-MA plasma current using an rf system. Plasma fueling is accomplished via gas puffing or possibly pellet or plasma gun injection.

During plasma operation the plasma impurities, including alpha particles, are removed using a limiter system and continuous vacuum pumping. The limiter consists of segments which form a continuous toroidal ring at the reactor outer midplane. The limiter is subjected to a peak heat flux of 4 MW/m^2 and is cooled with 150°C water which is used for feedwater heating. As particles impinge on the limiter, ~30% are directed into a slot behind the limiter. These particles are then pumped through a vacuum plenum region between the blanket and shield into 24 vacuum ducts at the top and bottom of the reactor. Forty-eight cryosorption/cryocondensation pumps are used. Twenty-four of the pumps are operated while the remaining twenty-four are rejuvenated. Pumps are rejuvenated hourly to minimize tritium inventory.

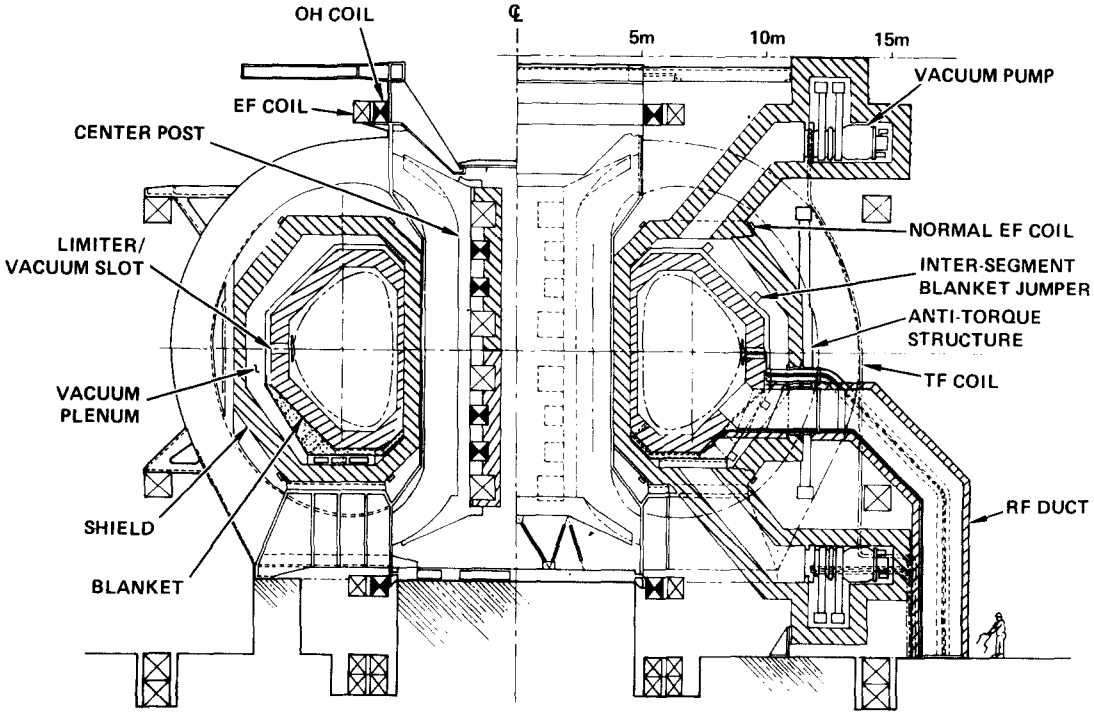

Fig. 3. STARFIRE reference design – cross-section.

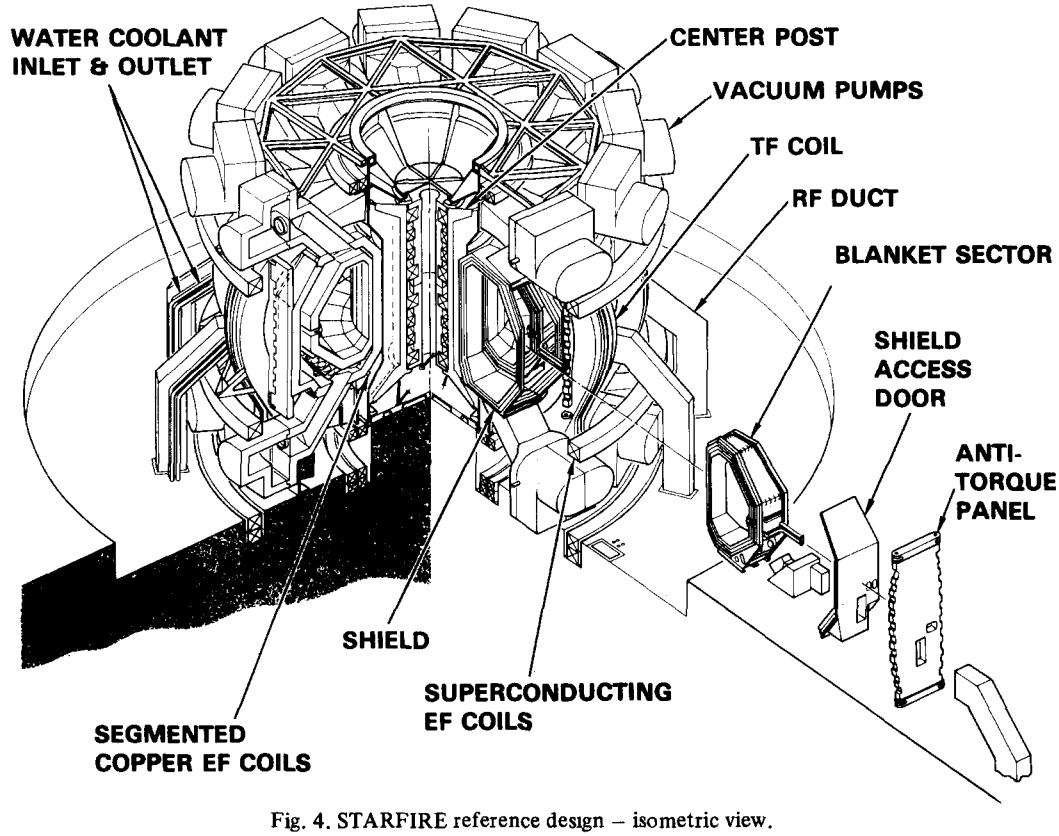

Fig. 4. STARFIRE reference design – isometric view.

The first wall is an integral part of the blanket structure. The blanket is segmented toroidally into 24 sectors to permit removal between TF coils. Two different sector sizes are used to permit location of the high-pressure coolant line disconnects outside the vacuum chamber. The first-wall and structural material is PCA stainless steel that operates at ~425°C maximum temperature when subjected to an average neutron wall load of 3.6 MW/m^2. The first-wall blanket is cooled by heavy water with inlet and outlet temperatures at 280°C and 320°C, respectively. This permits operation of the $LiAlO_2$ solid breeder material within a broad temperature range to enhance tritium release without sintering. A helium purge stream is used to extract the tritium.

The first-wall/blanket sectors also provide mounting for the 12 ECRH and 12 lower-hybrid waveguides, the fueling ports, and the limiter system. The waveguides and fueling ports are located on the sector between TF coils. The first wall, limiter, and waveguides are coated with beryllium to minimize the effects of sputtered impurities on the plasma. The first wall/blanket, limiter, and waveguide assembly are designed for a 20 MW-yr/m^2 life. Blanket sectors are manifolded separately to permit leak detection and islolation.

The shield provides neutron and gamma-ray attenuation and serves as the primary vacuum boundary for the plasma. The shield is assembled from 12 sectors and 12 shield rings. Dielectric breaks are located in six sof the shield rings near the outer surface of the shield to limit the radiation dose to 10^{10} rads. The Kapton dielectric seal is factory installed and designed for life-of-plant operation. Removable shield doors are located between TF coils to permit blanket sector removal. The shielding is ~1-m thick to reduce the gamma dose level to $<10^8$ rads so that elastomer door seals can be used. Redundant seals and dielectric breaks are used to permit leak detection and isolation.

The reactor magnet system consists of 12 TF coils, 8 superconducting EF coils, 4 normal conducting EF coils, and 6 OH coils. Two of the OH coils are combined with the EF coils to simplify assembly. No intertwined superconductors are used and the normal coils are segmented to permit maintenance. The TF coils have a common vacuum dewar at the inner coil leg and separate vacuum dewars on the outer leg. TF coil overturning moments are reacted through the 4 K center post and room temperature shear panels between adjacent TF coil outer legs. The room temperature TF coil case also supports the EF coils and the shield assembly. The vacuum pumps utilize an additional support frame.

Table 2
STARFIRE major design features

Net electrical power (MW)	1200
Gross electrical power (MW)	1440
Fusion power (MW)	3490
Thermal power (MW)	4000
Gross turbine cycle efficiency (%)	36
Overall availability (%)	75
Average neutron wall load (MW/m^2)	3.6
Major radius (m)	7.0
Plasma half-width (m)	1.94
Plasma elongation (b/a)	1.6
Plasma current (MA)	10.1
Average toroidal beta	0.067
Toroidal field on axis (T)	5.8
Maximum toroidal field (T)	11.1
No. of TF coils	12
Plasma burn mode	Continuous
Current drive method	rf
Plasma heating method	rf
TF coils material	Nb_3Sn/NbTi/Cu/SS
Blanket structural material	Austenitic steel (modified, PCA)
Tritium breeding medium	Solid breeder
Wall/blanket coolant	Water
Plasma impurity control	Low-Z coating + limiter and vacuum system + enhanced radiation + field margin
Primary vacuum boundary	At inner edge of shield

3. Key reactor design features

The following subsections describe certain highlights of the reference STARFIRE reactor design. Emphasis is placed on the rf current drive systems, the limiter/vacuum system, and the first-wall/blanket/shield system.

3.1. Plasma current drive and heating

In the time since the earliest proposal [3] to create a steady-state tokamak with wave-driven currents, the lower hybrid wave has received the most extensive study [4,5], and on this basis it was selected for the STARFIRE design. Theory indicates the local wave-power dissipation and current density are related as

$$\frac{P_{\mathrm{LH}}}{j} \alpha\, n_e n_1^2 \left[1 + \frac{\Delta n}{n_1}\right],$$

where n_e is the local electron density and where the

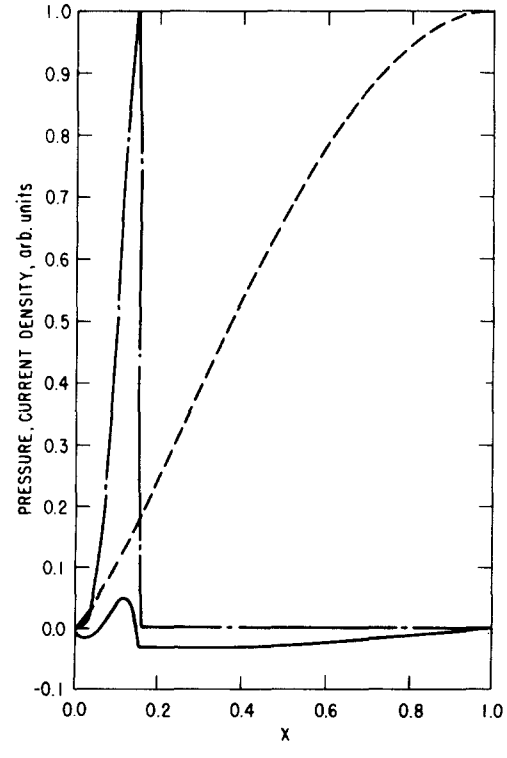

Fig. 5. Equilibrium pressure (dashed), toroidal (chain-dash), and poloidal (solid) current density.

antenna broadcasts wavelengths in the toroidal direction with a spectrum characterized by an index of refraction in the range n_1 to $n_1 + \Delta n$. Consequently, for a given current density, the rf power is reduced by generating current in low-density plasma, and by radiating a narrow band spectrum with low n_1. Obviously, the rf power is also minimized by operating with the lowest plasma current possible.

A plasma equilibrium was selected which meets our criteria; the total current is only 10 MA, and the current density is peaked near the plasma surface, in the region where the electron density is low. This equilibrium was tested for ideal MHD stability with the ERATO [6] and BLOON [7] codes. For the aspect ratio ($A = 3.6$) and elongation ($\kappa = 1.6$) characterizing the D-shaped plasma cross section of STARFIRE, the plasma was found to be stable to at least the design value of $\beta_t = 0.067$ against interchange, ballooning, and low-mode number kinks, provided the blanket reproduces the effect of a close-fitting conducting jacket around the plasma. The safety factor profile is monotonic so the resistive double-tearing mode is not a problem. For a fixed β_t, operation at high temperature and low density is desirable since the rf power is proportional to n_e [5]. We assume operation will occur in the hot mode [10] with $\bar{T}_e = 17$ keV, $\bar{T}_i = 24$ keV, and $\bar{n}_e = 1.2 \times 10^{20}$ m^{-3}. Additionally, the temperature profile is assumed to be fairly broad (corresponding to rf heating near the surface) while the density profile is quite narrow, further reducing n_e in the edge region where the current density is peaked.

The calculation of lower hybrid wave propagation and damping determines the values of n_1, Δn, and minimum required rf power, P_{rf}, to achieve 10 MA of current with a depth of penetration corresponding to that of the surface current equilibrium. The wave frequency is set at twice the local lower hybrid frequency at the deepest point of wave penetration, to avoid parametric instability, and n_1 is set equal to the minimum allowed by the accessibility criterion [8]. For the STARFIRE density profile, the antenna must deliver $P_{rf} = 63$ MW at 1.4 GHz with $n_1 = 1.20$, and $\Delta n = 0.62$. Fig. 5 displays the pressure and current density profiles as calculated from a cylindrical equilibrium model.

The Brambilla waveguide array [9] is ideally suited for current drive applications. The travelling waves are launched by phasing adjacent guides by 120 deg. Thus, three guides, each with a narrow opening (in the toroidal direction) of 4.0 cm and with 0.7 cm of metal septum, define the average wavelength in the toroidal direction. The spectral width, Δn, is established by limiting the number of guides (in the toroidal direction) in one array to thirteen. The vertical guide dimension is 20 cm, in order to transmit the TE_{10} mode, and eight banks of these arrays are stacked in the poloidal direction, forming a 0.62 m × 1.78 m module. One module is situated between each of the twelve toroidal field coils of the reactor. Averaged over the total antenna area, the wave intensity at the plasma may reach as high as 1 kW/cm^2. Higher intensity could possibly result in nonlinear plasma response, although the plasma physics of this point is not well understood. At these modest power levels, multipactor breakdown is not a concern.

The power supplies and rf system elements are located outside the reactor building. These elements are connected to the reactor by 12 rf duct assemblies that have 104 slots in each duct. The duct assembly will be mounted to the blanket sector as shown in fig. 6. The duct will be constructed from PCA stainless steel. PCA stainless steel was chosen because it is being used in a similar environment in the first wall. Welds near the plasma will be minimized by using a machined part within ~5 cm of the first wall. The interior of the steel ducts is coated with copper to minimize the power losses through the guide. Near the first wall, an additional coating of beryllium is added to the copper to minimize the effects of sputtered impurities.

The grill assembly will be cooled by 40°C water. The maximum structural temperature is ~310°C. The grill assembly protrudes through the shield door where a mechanical disconnect is located that permits removal of the directional coupler and rf window as part of an elbow. Removal of the elbow permits access to the blanket/shield for maintenance. A window is included in the duct elbow to prevent electron cyclotron breakdown in the slots. The TF coil field profile requires the window to be within 3 m of the TF coil leg. The window material is sapphire (alumina), which has been shown to withstand 10^{21} n/cm^2 before serious degradation occurs. Neutronics analysis has indicated this fluence will be reached in 10 yr of reactor operation. This indicates that win-

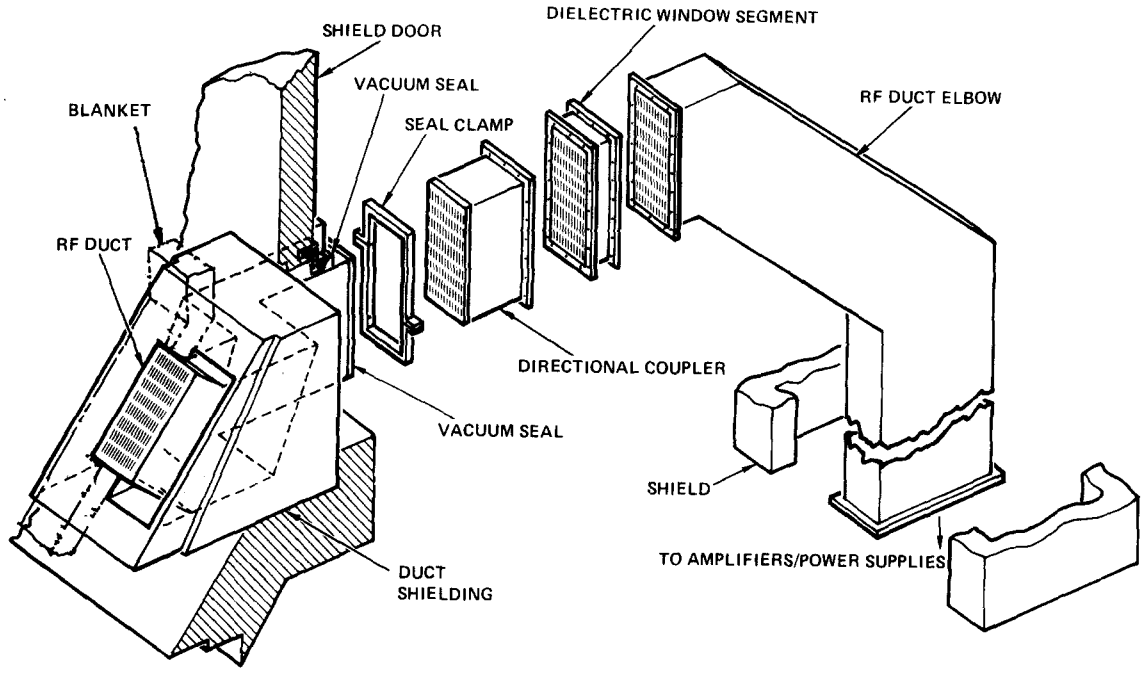

Fig. 6. Waveguide system, including Brambilla array at reactor wall.

dow replacement at the 6-yr blanket replacement interval is appropriate. A second window is located at the reactor building wall to provide an additional barrier against inadvertant breach of containment.

The power flow in the rf system is determined both by the power reflected back into the waveguides from the plasma and by the losses in the system hardware. The theory of the Brambilla array predicts the reflection coefficient for each waveguide in an array, which is a function of the electron density near the waveguides. We have assumed a simple model of the edge density, assuming a vacuum from the quide openings out to a distance, δ, beyond which the density increases linearly, with $\nabla n_e = 1.0 \times 10^{11}$ cm^{-4}. It may

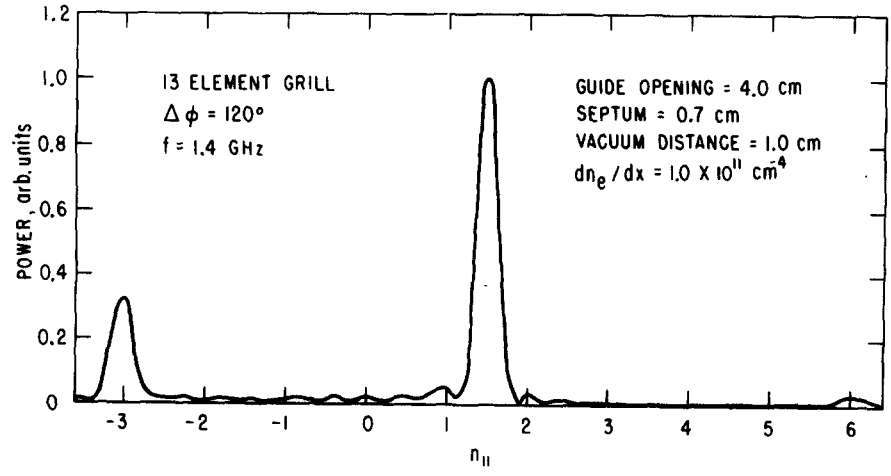

Fig. 7. Lower-hybrid wave spectrum, including sidebands.

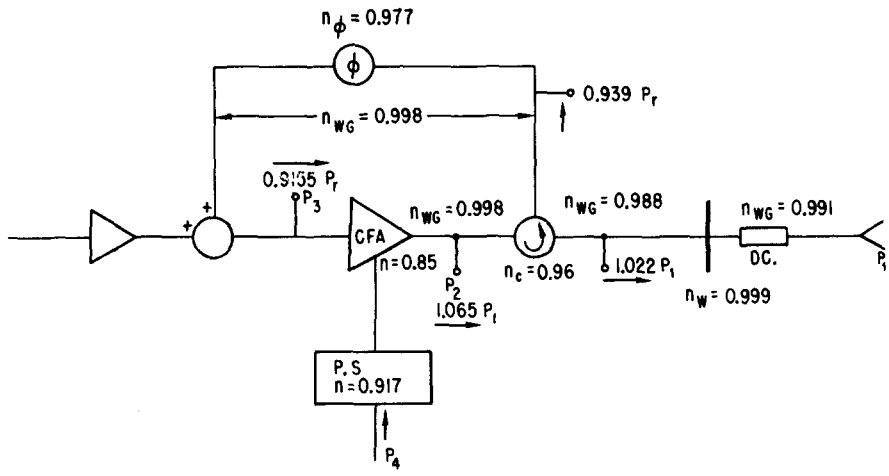

Fig. 8. Power flow diagram for rf system with reflected power recovery, assuming a tube development program; efficiencies indicated by quantity 'n'.

be necessary to place small secondary limiters of width ~δ near the antenna modules in order to tailor the electron edge profile for optimum coupling. While decreasing δ reduces the reflected power, it also puts a larger portion of the radiated power into spectral sidebands (see fig. 7). These sidebands, generated by wave interference, do not drive significant current and merely represent a sink of rf power, so their presence is unwelcome.

For the required P_{rf} = 63 MW to drive currents, enough power is lost to the sidebands when δ = 1.6 cm that a total P_{WG} = 110 MW must be absorbed in the plasma.

Fig. 8 diagrams the power flow and attenuation for the rf system. Waveguide and window losses are insignificant, with the circulators and phase shifters representing larger losses. For the substantial reflection coefficients encountered by the Brambilla array, it is important to directly recover the returning power, and crossed-field amplifiers (amplitrons or magnetrons) appear to be the tubes best suited to our needs [10]. These low-gain amplifiers offer high efficiency operation at a rating of a few hundred kilowatts. With a development program, it seems probable that the plasma current in STARFIRE can be driven with less electrical power than the reference value of 150 MW.

The burn cycle envisioned for STARFIRE consists of four phases. Breakdown is accomplished by pulsing clean deuterium-tritium gas into the previously evacuated torus and applying ~3 MW of ECRH power for ~1 s. This ionizes and heats the plasma to several hundred eV temperature level. Next, the previously charged, superconducting OH coil is discharged through a dump resistor, thereby inducing ~1 MA of plasma current. The next period (60 s) is the main current ramp and heating phase. The lower-hybrid rf drive is applied to the plasma and slowly increased up to full power. This gradually heats the plasma and brings the current up to the full value of 10 MA in 60 s. During the entire startup period, the EF current is gradually raised to its full value, in order to keep the plasma in MHD equilibrium. The required EF power, which is supplied through a rectifier/invertor SCR supply, is low enough to be taken off the grid without need of on-site electrical storage. The plasma burn period is of the order of 6 mo to 1 yr, depending on required shutdowns for maintenance operations. During the burn, rf is applied continuously and small variations are made in the inside copper EF coils to control the plasma position. Thermal control of the plasma is maintained by small variations in the rf power and small amounts of injected impurities (e.g. xenon). Normal shutdown is accomplished by stopping the refueling, reducing the rf power, and gradually letting the plasma current decay. An emergency shutdown capability is also planned to shut down the plasma in ~3 s.

3.2. Impurity control, vacuum and tritium systems

3.2.1. General considerations

The impurity control, vacuum, and tritium systems are strongly interrelated. The STARFIRE strategy has been to develop these systems so as to satisfy the following goals: (1) have manageable heat loads in the medium where the alpha and impurity particles are collected; (2) have a reasonable and reliable vacuum system that minimizes the number and size of vacuum ducts; (3) have a high tritium burnup to minimize the tritium inventory in the fuel cycle; and (4) have engineering simplicity compatible with ease of assembly/disassembly and maintenance.

The impurity control system for STARFIRE uses a limiter/vacuum system together with a beryllium coating on the first wall and limiter. In addition, the toroidal field coils are designed with enough field margin to accommodate a moderately high concentration of helium in the plasma. In order to minimize the heat load to the limiter, most of the alpha-heating power to the plasma is radiated to the first wall by injecting a small amount of xenon along with the deuterium–tritium fuel stream. The xenon atoms result in enhanced line-and-recombination X-ray radiation over most of the plasma volume. The helium removal efficiency of the limiter/vacuum system is intentionally kept fairly low for two reasons: (1) to ease the limiter design; and (2) to minimize the tritium inventory tied up in the vacuum system.

Previous conceptual design studies have shown that requiring very high removal efficiency of the alpha particles and impurities from the plasma results in a complex vacuum system with a large number of large size vacuum ducts. This causes substantial neutron and gamma-ray streaming which results in concern about radiation effects in the vacuum pumps as well as other reactor components; the need for substantial shielding of the vacuum ducts, pumps, and other components; and activation of a large volume of materials. Furthermore, a complex vacuum system with enhanced radiation complicates reactor maintenance. The complexity of the vacuum system can be eased considerably by requiring a low helium removal efficiency. A removal efficiency as low as 10% is normally sufficient for a moderate helium equilibrium concentration in the plasma to permit steady-state ignited plasma operation. For fixed plasma beta, geometry, and fusion power, the increase in plasma pressure due to the alpha and impurity particles is compensated for by an increase in the magnetic field (field margin). Coating all surfaces exposed to the plasma by a low-Z material is necessary to keep the field margin to an acceptable level. Lower-particle removal efficiency implies higher tritium recycling and fractional burnup.

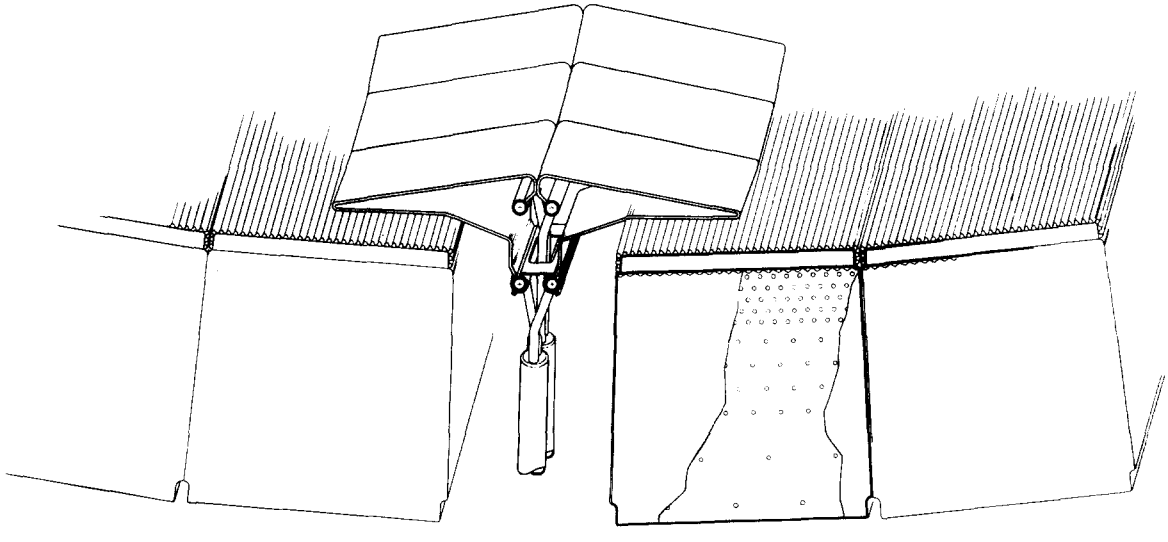

Fig. 9. Limiter arrangement.

The three approaches described above (enhanced plasma radiation, low-Z coating and low-particle removal efficiency) can be adapted to improve almost any impurity control/plasma exhaust system with varying degrees of success. In contrast, the engineering complexity and impact on reactor maintainability vary strongly from one impurity control concept to another. The presently known concepts for the different types of divertors and divertorless systems were evaluated. It has been concluded that the reactor engineering requirements are best satsified by the limiter/vacuum system. The system shown in fig. 9 utilizes a toroidal limiter, centered at the midplane, for concentrating the alpha particles and impurities diffusing out of the plasma. The limiter consists of a front face, two 'leading edges' and a slot region formed between the leading edges and the first wall. The slot region leads into a limiter duct region that penetrates through the blanket and opens into a plenum region. The plenum region is of sufficiently large size so that it provides for spreading the radiation leakage from the limiter duct into a larger surface area of the bulk shield; and the conductance of the plenum region is large enough to permit locating the vacuum ducts in the bulk shield sufficiently removed from the midplane that radiation streaming from the limiter duct in the blanket to the vacuum pumps is acceptable. Table 3 presents a summary of the major features of the limiter/vacuum system and the following subsections present more details about the system.

3.2.2. Scrapeoff zone physics

The function of the limiter is to concentrate all of the charged particles diffusing out of the plasma, and to permit removal of some of them. The tip of the limiter, on the front face, defines the start of the plasma-edge region or 'scrapeoff zone'. The charged particle flux in the scrapeoff zone and hence to the limiter falls off as e^{-x/δ_p} where x is the distance from

Table 3
Major features of the limiter/vacuum system

Helium production rate (s^{-1})	1.24×10^{21}
Helium reflection coefficient, R_α	0.75
Hydrogen reflection coefficient, $R_{D,T}$	0.90
Alpha particle concentration, n_α/n_{DT}	0.14
Beryllium (low-Z coating) concentration, n_{Be}/n_{DT}	0.04
Toroidal-field margin at plasma center (T)	0.85
Scrape-off region thickness (m)	0.2
Limiter (one toroidal limiter centered at midplane)	
Structural material	tantalum alloy
Low-Z coating material	beryllium
Coolant	water
Coolant inlet temperature (°C)	135
Coolant outlet temperature (2 pass) (°C)	165
Maximum coolant pressure, MPa (Psia)	2.8 (400)
Total heat removed from limiter (MW)	200
(90 MW transport, 56 MW radiation plus neutrals and 54 MW nuclear)	
Maximum heat load (at leading edge) (MW/m^2)	4
Coolant channel size	8 mm × 4 mm
Wall thickness (mm)	1.5
Ratio of maximum effective stress to the allowable	0.9
Maximum material temperature (coolant side) (°C)	235
Maximum material temperature (coating side) (°C)	350
Maximum nuclear heating rate (MW/m^3)	79
Atomic displacements (dpa/yr)	14
Helium production rate (appm/yr)	<5
Hydrogen production rate (appm/yr)	37

the tip and δ_p is the e-folding distance for particles.

The value of δ_p can be estimated by considering a particle that, on its orbit around the torus, has just missed hitting the limiter tip. In order to return to the vicinity of the limiter, the partial must make one revolution poloidally and q revolutions toroidally, where q is the safety factor at the plasma edge. In doing so, the particle diffuses outward in minor radius and hits the plasma at an average (root mean square) distance of δ_p from the tip. This distance is given by $\delta_p = \sqrt{D_\perp \tau}$, where $D_\perp$ is the diffusion coefficient characteristic of the edge region, and τ is the 'flight time' for the particle to return to the limiter. For a path length L, and for a velocity $V_{/\!/}$, along the field line, $\tau = L/V_{/\!/}$. Using a Bohm diffusion coefficient (with an ion mass of 2.5 amu):

$$D_\perp(\mathrm{m^2/s}) = 0.0625 \frac{T_e(\mathrm{eV})}{B(T)}, \tag{1}$$

gives

$$\delta_p(\mathrm{m}) = 3.176 \times 10^{-3} \sqrt{L/B}\, T_e^{1/4}. \tag{2}$$

For the STARFIRE limiter system, $L = 2\pi R_L q$ where $R_L = 9$ m is the major radius of the limiter and $q = 5.1$, giving $L = 288$ m. Using the value of $B_0 = 5.8$ T in the plasma center as an average B for use in eq. (2) and using an edge temperature of $T_e = 600$ eV, then gives a value of $\delta_p \approx 10$ cm for the particle e-folding distance.

Based on the consideration that the plasma temperature in the scrapeoff zone may fall off at the same rate as the particle flux, then the energy or power flux, which is proportional to the product of density and temperature, should fall off at twice this rate, i.e. as e^{-x/δ_E}, where $\delta_E = 1/2\ \delta_p$ is the energy e-folding distance. The particle transport power to the limiter is 90 MW. Based on this value and the limiter geometry, the power flux to the limiter is given by:

$$q = 16 \sin\theta\ e^{-x/\delta_E}\ (\mathrm{MW/m^2}), \tag{3}$$

where θ is the angle that the poloidal field line (which is nearly vertical at this location) makes with the limiter, and $\delta_E = 5$ cm.

3.2.3. Limiter design

The limiter/vacuum system uses a toroidal limiter, 1 m high, centered at the midplane and located at the outer periphery of the plasma. The toroidal limiter consists of 56 sectors. Each sector has a mushroom-shaped cross section that consists of symmetrical top and bottom flat ribbon sections joined to the coolant

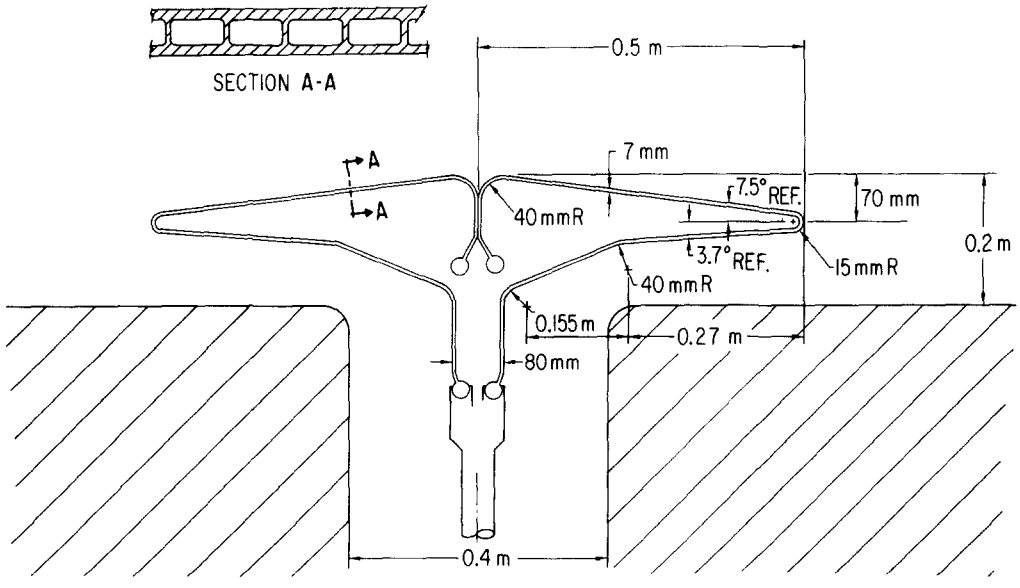

Fig. 10. Schematic of limiter design showing dimensions.

inlet and outlet headers. The mechanical design is shown in fig. 9 and the limiter and coolant channel dimensions are given in fig. 10.

The heat load on the limiter consists of three components: (1) transport power flux given by eq. (3); (2) heat flux from plasma radiation and neutrals ~0.9 MW/m^2; and (3) volumetric nuclear heating of ~40 MW/m^3. A maximum surface heat load of 4 MW/m^2 occurs at the two leading edges (one at the top and one at the bottom) where $\theta = 0$. Moving the leading edge closer to the first wall reduces the peak heat load but also reduces the number of alpha and impurity particles that can be pumped. The location of the leading edge at $x = 7$ cm was determined from a tradeoff analysis.

A detailed assessment of material candidates that included radiation effects, thermal-hydraulics, and stress analyses was performed. The relatively high surface heat load and the intense radiation environment require a structural material with good thermomechanical properties and resistance to radiation damage. The use of liquid metal coolants permits several excellent structural materials, particularly the refractory alloys, to be considered. Since liquid metals were excluded because of perceived safety problems, only water offers an attractive limiter coolant. The choice of water as a coolant limits the structural material options somewhat. These options will be discussed in some detail shortly. A tantalum alloys is selected as the primary structural material with vanadium and copper alloys as backup options. Both tantalum and vanadium permit useful heat recovery for energy conversion while with copper the permissible coolant pressure and temperature are so low that useful heat recovery is not feasible.

The water coolant speed is taken as ~8 m/s to assure a heat transfer coefficient of $\geqslant 10^4$ Btu/hr-ft^2 °R. In addition, liquid subcooling of 55°C is assumed to prevent transition from subcooled nucleate boiling to film boiling at the leading edge. The coolant temperature rise and pressure drop per pass are 15°C and 0.2 MPa, respectively. The design is based on a double pass (two sectors) with coolant inlet temperature of 135°C into one sector and a coolant exit temperature from the adjacent sector of 165°C. The maximum (inlet) coolant pressure is 2.8 MPa. The 200-MW heat from the limiter is used for feedwater heating in the power conversion cycle.

The critical area of the limiter from a thermal stress standpoint is the leading edge which receives the highest surface heat flux. The design of the leading edge must ensure that stresses are low enough to preclude failure over the lifetime of the limiter. Detailed stress analysis shows that the maximum effective stress due to combined temperature effects and coolant pressure is ~315 MPa at the leading edge for a limiter outer wall thickness of ~1–1.5 mm. This is ~90% of the allowable stress for TA-10W.

3.2.4. Limiter materials

The limiter structural material must withstand a strenuous set of operating conditions. It must be capable of withstanding a high surface heat flux in a high neutron field, and it must be chemically compatible with the water coolant and plasma environment. In order to extract useful heat from the limiter, the structural material must also possess adequate high-temperature strength. The lifetime of the limiter should be equal to that of the first wall and blanket. Several materials, which can potentially withstand the peak heat flux, have been evaluated for uses as the limiter material.

Several materials can be eliminated from consideration because of one or more unacceptable properties. Pure copper is known to exhibit a high degree of swelling in the range of 200–400°C [11], and it rapidly loses its strength above 200°C. Alloying is likely to reduce the swelling and to increase the strength in copper, but the improvement would be offset by a significant decrease in thermal conductivity [12]. These properties limit the use of copper and copper alloys to low temperatures where useful heat recovery is not possible. Even though low temperature operation of copper is possible, the high swelling reported in pure copper would result in an unacceptably short lifetime. Both tungsten and molybdenum are extremely susceptible to an increase in the ductile-brittle transition temperature (DBTT) with irradiation [13,14] and both materials are difficult to fabricate. The resulting low ductility with irradiation in tungsten and molybdenum has eliminated them from consideration.

The remaining materials, tantalum, vanadium, and niobium, are susceptible to corrosion in high-temperature water and to hydrogen embrittlement. The maximum operating temperatures of these materials

are determined by their reactions with the environment and not by the loss of strength with temperature or the effects of radiation. Vanadium alloys are the most resistant to radiation damage, but they have the lowest thermal stress resistance of the materials considered. The response of niobium and tantalum to radiation and the chemical environment are expected to be similar, but tantalum alloys exhibit a superior thermal stress resistance.

From these considerations, tantalum and vanadium alloys appear to have the greatest potential as limiter materials. Based upon its ability to withstand higher heat fluxes and its adequate properties in other areas, tantalum has been selected as the first choice for the limiter material with vanadium as the backup. The primary concerns in the use of tantalum are the effects of radiation and corrosion. The limited available data indicates that tantalum alloys should be resistant to water corrosion for temperatures $<250^{\circ}$C [15]. The effects of hydrogen from the plasma on tantalum should be minimal since the equilibrium value of hydrogen concentration at 250°C and 10^{-3} torr hydrogen pressure (the maximum pressure envisioned) is only ~40 wppm. This concentration is substantially below that required to embrittle the material at room temperature. In addition, it is expected that the low-Z coating and/or the oxide layer on the tantalum surface will act as a barrier to hydrogen permeation. In order to avoid hydrogen permeation from the coolant, the water chemistry should be carefully controlled. Radiation swelling in tantalum is not expected to be a problem at the lower operating temperatures of the limiter, but there is some evidence that tantalum is embrittled by irradiation [13]. Radiation embrittlement represents the most serious concern to the successful operation of a tantalum limiter, although it is not clear whether this embrittlement is due entirely to neutron radiation or whether interstitial contamination also contributes to the embrittlement. If, in the future, the embrittlement proves to be an insurmountable problem then a vanadium alloy would be selected as the limiter material.

3.2.5. Vacuum system

The STARFIRE vacuum system is designed to minimize neutron streaming while still providing adequate pumping. It consists of the following components (see fig. 3): the two limiter slots, the limiter duct, the plenum region, the vacuum ducts, and the vacuum pumps. The limiter slots (fig. 10) are defined as the 0.1-m gap between the back of the limiter and the first wall. The limiter duct is 0.4 m in height and it extends through the 0.7-m blanket and shield to the plenum region. The plenum region is the space between the blanket and the shield and is 1.0 m in width (approximately 20 cm is used for coolant manifolding) and approximately 12 m high. The limiter slots, the limiter duct, and the plenum extend circumferentially around the outside of the torus. There are 24 vacuum ducts 6 m long $\times$ 1.0 m diameter and 48 compound cryopumps (24 on-line at any given time), each with a helium speed of 120 m^3/s.

Based on the equations derived for particle and energy flux in the scrape-off region, and on the limiter dimensions, as shown in fig. 10, the front face of the limiter will receive about 60% of the particle flux and 80% of the energy flux. The slot region will receive about 30% of the particle flux, the remaining 10% going to various parts of the first wall. The particle flux consists of the deuterium–tritium ions, helium ions, beryllium ions originally sputtered from the coating, and electrons. The ions of all species that hit the front face of the limiter, are neutralized and return to the plasma (although they may recycle quickly from the plasma edge). The only particles that can be pumped are the 30% entering the slots. Fortunately it appears that almost all of the helium entering the slot will be pumped.

The helium ions entering the slot region are neutralized on the back limiter surfaces. Some of the helium atoms are scattered directly into the vacuum slot where they are eventually pumped. Helium atoms traveling back up the slot (whether coming directly from the limiter or recycling from the vacuum system) are nearly all ionized by the incoming stream of hot electrons. Once ionized, they are accelerated back to the limiter by the pre-sheath electric field that is set up in the slot region. An additional mechanism [16,17] for trapping helium may also be the collisions between helium atoms and the incoming ions. It is also possible that the plasma streaming into the limiter will maintain a pressure gradient which may help trap the helium. For these reasons the trapping, or 'inversion probability' κ of helium should be nearly unity, although the exact values require further analysis.

On the other hand, hydrogen trapping in the slot region should be much less. This result is due to the fact that while helium does not charge-exchange at these temperatures deuterium–tritium neutrals can be ionized by electrons and can also charge-exchange (cx) with deuterium–tritium ions with about equal probability. Although the ionized deuterium–tritium will be trapped, like helium, the neutrals created from cx (or from a sequence of cx events) can escape. Therefore, the inversion probability for deuterium–tritium will be much lower than for helium.

The reflection coefficient, R, for species i, is given by $R_i = 1 - F\epsilon_i$, where F is the fraction entering the slot and ϵ is the transmission probability.

Table 4 lists the vacuum system conductances and the reflection coefficients for deuterium-tritium and helium using analytical formulas for the various conductances and for inversion probabilities of $\kappa_{He} = 0.95$, $\kappa_{DT} = 0.5$, and F = 0.3. The conductances of both the limiter duct and the plenum region are two orders of magnitude greater than that of the vacuum ducts in the bulk shield. The speed of the compound cryopumps is an order of magnitude greater than the conductance of the vacuum ducts. The effective conductance of the vacuum system (490 $m^3 s^{-1}$) is therefore very dependent on the geometry of the vacuum ducts. A Monte-Carlo calculation was also used to determine the transmission probability and these results are shown in fig. 11. As shown, the Monte-Carlo results agree well with the analytical calculation. The Monte-Carlo calculations also showed that ϵ was sensitive to the vacuum duct diameter. Monte Carlo calculations made by Seki et al. [18] for a poloidal divertor channel, with similar geometry also show similar results.

Table 4
STARFIRE limiter/vacuum system

Limiter slots conductance, C_l	3700 $m^3 s^{-1}$
Limiter duct conductance	17 000 $m^3 s^{-1}$
Plenum conductance	25 000 $m^3 s^{-1}$
Vacuum ducts conductance	620 $m^3 s^{-1}$
Total helium pump speed	2900 $m^3 s^{-1}$
Effective conductance, C_R	490 $m^3 s^{-1}$
Conductance ratio, $\gamma = C_l/C_R$	7.6
Particle fraction into limiter slots, F	0.3
Inversion probability, κ, helium	0.95
Transmission probability, ϵ, helium	0.8
Reflection coefficient, R, helium	0.75
Inversion probability, κ, deuterium–tritium	0.5
Transmission probability, ϵ, deuterium–tritium	0.3
Reflection coefficient, R, deuterium–tritium	0.9
Fractional burnup, tritium	0.35

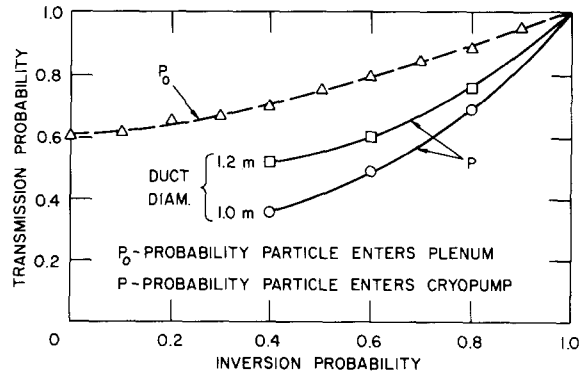

Fig. 11. Limiter/vacuum system Monte-Carlo calculation.

The reflection coefficients listed have the following implications. At equilibrium, the removal rate of helium by the limiter/vacuum system is equal to the generation rate by fusion. For the STARFIRE parameters, and for $R_{He} = 0.75$, this gives a helium concentration of ~14% of the deuterium-tritium density. The large value of R_T (also R_D) results in a very high fractional burn, ≥ 0.35, in the plasma. Thus, the tritium fuel is efficiently used.

The vacuum concept satisfies the design objectives. The limiter/vacuum concept appears to preferentially remove helium from the system, and thus reasonable purity control is achieved while maintaining a very high fractional burnup of tritium (35%). The geometrical configuration was chosen such that conductance is maximized while neutron streaming is minimized.

3.2.6. Tritium considerations

As noted above, the limiter/vacuum system achieves a very high fuel utilization efficiency, having a tritium fractional burnup of 35%. As a result, tritium flow rates in the fuel cycle (table 5) are very low, about 1 kg/day, or 250 g/GWth-day. By comparison, most previous reactor designs have a much

Table 5
Tritium parameters

Mass flow rates	
Fractional burnup (%)	35
Tritium burned (g/day)	530
Tritium fueled (g/day)	1510
Tritium exhaust (g/day)	980
Tritium bred (g/day)	560

Tritium inventories (g)

	Vulnerable	Not vulnerable
Solid breeder	—	5000–10 000
Purge stream	0.2	—
Tritium recovery	200	—
Vacuum pumps	150	—
Fueling	< 50	—
Fuel processing	—	100
Storage	—	1000
Total	<400	6000–11 000

lower fractional burnup, 1-10%, and the corresponding fuel cycles have to process 1-10 kg/GWth-day. Clearly there is a strong incentive to maximize fractional burnup.

The fuel cycle scenario (fig. 12) illustrates the major tritium handling components, their functions, and their logical locations. Vacuum pumping, tritium breeding and recovery, and plasma fueling components are all physically located in the reactor building. Fuel reprocessing components are located in a separate tritium facility building, as noted in fig. 12. The components in fig. 12 have been analyzed and the tritium holdups estimated. Of particular importance to reactor safety are those components which have the potential for accidental release of a significant portion of their tritium inventory. Accordingly, inventories in these components are defined as 'vulnerable' tritium inventories (table 5). For example, the tritium in the solid breeder is held rather tenaciously and since the breeder does not have

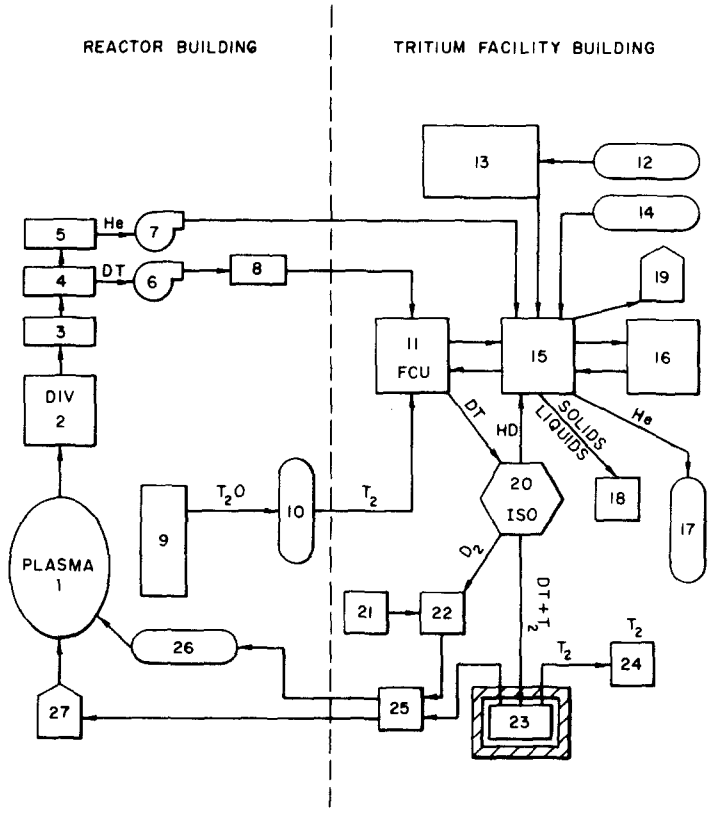

Fig. 12. Tritium fuel cycle scenario for STARFIRE.

the potential for vigorous exothermic chemical reactions, it is relatively nonmobile; and although there is a large inventory in the solid breeder (5–10 kg), the probability of release is very small. Similarly, the stored tritium is kept in a barricaded storage vault and is not considered to be vulnerable. Fuel processing components are located in gloveboxes and secondary containments in the separate tritium facility building, and are also relatively nonvulnerable. By contrast, fracture of a cryopump or a line leading from such a pump could potentially release its tritium inventory to the reactor building. There are emergency air detritiation systems designed to process the atmosphere within the reactor building and remove the tritium in a timely fashion. The vulnerable and nonvulnerable tritium inventories are listed in table 5. The total vulnerable inventory is less than 400 g, or <100 g/GWth. Because of the high tritium fractional burnup, and the efforts made to design components for minimum vulnerable tritium inventory, this number is very low in comparison with other reactor designs.

3.3. First-wall/blanket design

The technological and design aspects of various first-wall/blanket concepts have been considered in the selection of a reference design for STARFIRE. The approach used in the present study involves the identification of key technological constraints of candidate tritium-breeding blanket concepts, establishment of a basis for assessment and comparison of the critical problem areas and design features of each concept, and development of a reference design for STARFIRE. Major emphasis has been placed on safety and environmental acceptability, with primary goals that include low tritium inventory in the blanket, minimal long-lived activation products and minimal stored energy. An *a priori* decision was made to focus the present study on concepts that utilize solid lithium compounds for the tritium-breeding material. The materials selection and design implications of the various first-wall/blanket components are summarized and the major design options that lead to the optimized design for STARFIRE are presented. Since the main function of the limiter and low-Z coating relates to impurity control, most aspects of these components have been discussed in the previous section.

3.3.1. Materials selection

The development of the reference STARFIRE first-wall/blanket design involved numerous tradeoffs in the materials selection process for the breeding material, coolant, structure, neutron multiplier, and reflector. With the limited scope of the present paper, only the major parameters and properties that impact materials selection and design criteria are discussed. Additional details are given in the STARFIRE design report [1]. Table 6 summarizes the primary candi-

Table 6
Candidate and reference first-wall/blanket materials

	Breeder	Coolant	Structure	Neutron multiplier	Reflector
A.	α-$LiAlO_2$	Pressurized water	Austenitic SS (adv. alloy)	Zr_5Pb_3	Carbon
B.	γ-$LiAlO_2$	Pressurized water	Ferritic steel	Be	D_2O/SS
	Li_2TiO_3			Zr	H_2O/SS
	Li_2SiO_3			BeO	ZrC
				Pb-Bi eut.	SiC
C.	Li_7Pb_2	Helium	Ti alloy	PbO	
	Li_2O		V alloy	Pb	
	Li_2ZrO_3		Ni alloy	Bi	

A – Reference material for STARFIRE.
B – Other primary candidate materials.
C – Materials assessed but not candidates for STARFIRE.

Table 7
Predicted temperature limits for adequate tritium release from solid breeding materials

Breeding material	Melting temp. (°C)	Unirradiated		Irradiated	
		T_{min} (°C)	T_{max} (°C)	T_{min} (°C)	T_{max} (°C)
Li_2O	1700	360	1000	410	910
$LiAlO_2$	1610	450	1000	500	850
Li_2SiO_3	1200	370	900	420	610 [a]
Li_2Si	760	430	550	480	420
LiAl	700	250	500	300	380
Li_7Pb_2	726	270	530	320	390

[a] 510°C if significant burnup of lithium occurs.

date materials considered for STARFIRE and indicates the materials selected for the reference design.

3.3.1.1. Tritium-breeding material. The STARFIRE study has focused on the use of solid tritium breeding materials; and hence, liquid lithium, liquid lithium alloys, and molten salts have not been considered. Important criteria considered in the selection of potentially viable solid breeding materials include chemical stability, compatibility, neutronics properties, and tritium release characteristics. The α-$LiAlO_2$ is selected on the basis of the best combination of these materials requirements. It is one of the most stable compounds considered and compatibility should not be a major problem. Adequate breeding is attainable with the aid of a neutron multiplier and the tritium release characteristics are nearly as good as any of the candidate compounds. The primary advantages of α-$LiAlO_2$ compared to γ-$LiAlO_2$ relate to the higher density, which will result in a thinner breeding zone, and the fact that α is the stable phase at temperatures below ~900°C. The major disadvantage of Li_2TiO_3 is a lack of data base. A slight potential advantage of this compound is its lower long-term activation compared to the aluminate. The silicate is similar to the above compounds, but because of its lower melting temperature its chemical stability and compatibility characteristics are not as good.

Table 7 summarizes the allowable operating temperature ranges for the candidate compounds that have been predicted from available thermodynamic data [19]. The low-temperature limits, which are defined by tritium diffusion kinetics in the solid, are based on very small (~1 μm) grain size. The upper temperature limits are based on sintering characteristics of the solids which would close interconnected porosity and increase the diffusion path. Allowances for radiation-induced trapping of tritium at the lower temperatures and radiation-induced sintering at the higher temperatures are indicated.

The ceramics are preferred over the intermetallic compounds for the reference solid breeding material because of the larger allowable operating temperature ranges. On the basis of this criterion, Li_2O and $LiAlO_2$ appear to have an advantage. However, the calculated solubility of tritium in Li_2O at these temperatures and at reasonable T_2O partial pressures in the tritium-processing stream ($>10^{-1}$ Pa) is much greater than 100 wppm. Since this concentration translates to more than 35 kg of tritium in the blanket, Li_2O is not considered a viable candidate.

3.3.1.2. Coolant selection. Coolant selection for STARFIRE focused primarily on the tradeoffs between water and helium. Liquid-metal coolants were not considered in the present study and, except for a lower operating pressure, molten salts have little advantage over water. Since this advantage is outweighed by the disadvantages of higher melting temperatures and greater compatibility problems, the salts are not considered prime candidates. Although steam was given some consideration, any advantages over pressurized water or helium are minimal. The characteristic advantages of pressurized water coolant over helium, which lead to the selection of pressur-

ized water for the reference coolant were discussed in section 2.1.

Heavy water (D_2O) has several advantages compared to H_2O. Processing of tritium from the water coolnat is less difficult for D_2O and deuterium leakage from the first-wall coolant into the plasma chamber is less detrimental than hydrogen. Another important advantage of D_2O relates to the lithium burnup and energy distribution in the solid breeder. As discussed in more detail in later sections, the D_2O gives a more uniform burnup and energy distribution. The major disadvantage of D_2O is its high cost. This led to the selection of H_2O.

3.3.1.3. Selection of the structural material. Six classes of materials generally considered as candidates for the first-wall/blanket structure are austenitic stainless steels, high-nickel alloys, titanium alloys, vanadium alloys, niobium alloys, and ferritic steels. Although the structural materials limitations were an important consideration in the selection of other blanket materials, the justification given here for the structural material choice is based on the specified coolant and breeder material. Nickel alloys are eliminated primarily on the basis of poor radiation damage resistance (embrittlement), no physical property advantage (thermal stress factor), and limited mechanical property advantage at temperatures required for water coolant. Titanium alloys are not considered viable candidates for the first-wall region because of their affinity for hydrogen. Vanadium and niobium alloys were eliminated because of their poor corrosion resistance in water and limited mechanical advantage at low operating temperatures.

The major focus has been on the tradeoffs between austenitic stainless steels and the ferritic steels. Table 8 summarizes the comparative advantage of an advanced austenitic stainless steel and a ferritic steel for the structural material. In addition to the design specific considerations listed in table 8, the major drivers in the selection of the austenitic stainless steel relate to its ease of welding, its nonmagnetic properties, and the potential increase in the DBTT of ferritic steel after irradiation.

3.3.1.4. Neutron multiplier. In order to achieve adequate tritium breeding with the primary candidate breeding materials, a neutron multiplier must be incorporated into the blanket. The most promising neutron multiplier materials are listed in table 6. The

Table 8
Comparative analysis of advanced austenitic stainless steel versus ferritic steel

Advantages of austenitic stainless steel
Ease of welding
– no post-weld heat treatment
– higher reliability
Mechanical properties less sensitive to composition and heat treatment
Lower DBTT
Lower corrosion mass transfer in water
Non-magnetic
Advantages of ferritic steel
Lower radiation swelling
Lower radiation creep
Better physical properties – thermal conductivity and thermal expansion
Moderately lower activation
Design specific considerations
Steady-state operation tends to reduce physical property (thermal stress factor) advantage of ferritic steel
Water coolant and lower structure temperature tends to reduce radiation damage advantage of ferritic steel
Long-term activation (>30 yr) results primarily from molybdenum (~1% in ferritic steel; 2% in austenitic steel)
Burnup of solid breeder poses additional blanket life time limitation

lead and bismuth are acceptable in most respects, but the lead-bismuth eutectic alloy is preferred to either lead or bismuth. The lead-oxide is less desirable because of its very low thermal conductivity, high mass (relatively large thickness required), and compatibility problems. The beryllium oxide is considered the optimum multiplier for concepts in which the multiplier is homogeneously mixed with the breeder. The primary concern with zirconium is the marginal multiplication. That for lead–bismuth is the fact that it is a liquid metal which has some compatibility problems at high temperatures. Beryllium provides high multiplication but is subject to radiation swelling and relatively high burnup, produces significant gas from transmutations, and produces relatively high burnup gradients in the blanket. A major advantage of beryllium is its light weight and relatively thin multiplier zone requirement. An attempt to find a material with the benefits of lead but which is solid at anticipated operating temperatures led to the consideration of the compound Zr_5Pb_3. Although the data base is limited, this material reportedly melts at 1400°C and has a calculated density of 8.9 g/cm^3.

3.3.1.5. Reflector. Primary candidates for the reflector are H_2O or D_2O contained in austenitic steel, graphite and carbides such as SiC or ZrC. The H_2O/stainless steel provides the thinnest reflector region. Graphite requires a thicker reflector zone but results in minimal activation products. With both the water and graphite, an austenitic steel with low molybdenum content is proposed to reduce long-term activation. Stable carbides are considered to mitigate the potential for carburization of the steel at high temperatures.

3.3.2. Design of blanket modules

Several design concepts have been considered for integrating the breeder, structure, coolant, neutron multiplier, and reflector into an optimized blanket design. The addition of each of these components significantly impacts the design and material compatibility problems that must be considered. Three blanket concepts were analyzed in the selection of the reference design for STARFIRE. The first concept utilizes a separate neutron multiplier zone between the first wall and the breeder region. The second concept utilizes a heterogeneous arrangement of several neutron multiplier and breeder regions behind the first wall followed by a separate breeder region. The third concept utilizes a homogeneous neutron multiplier/breeder region directly behind the

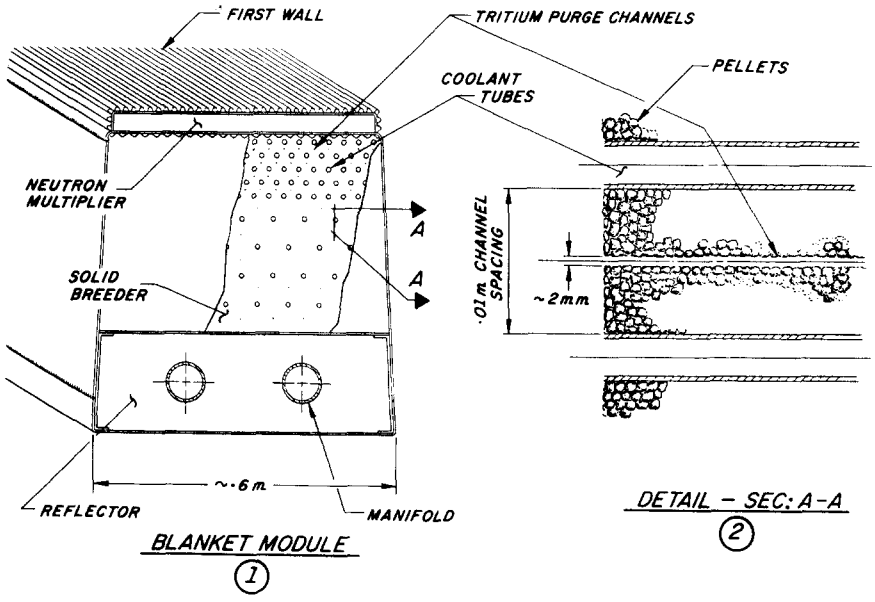

Fig. 13. Schematic diagram of STARFIRE blanket concept.

first wall followed by a separate breeder region. This last concept requires compatible breeder/multiplier materials, which probably limits the multiplier to beryllium oxide. Similar first-wall and reflector designs are proposed for all three concepts. The second concept is more complex from a design point of view and probably requires a larger structural fraction to separate the breeder regions from the multiplier regions. The first concept with the separate multiplier region is selected for the reference design, primarily because a more uniform lithium burnup and energy generation rate can be obtained in the blanket. This advantage allows longer blanket life before changeout and simplifies the heat transfer problems.

Fig. 13 is a schematic diagram of the blanket cross section showing the water-cooled austenitic stainless steel first wall, the Zr_5Pb_3 neutron multiplier zone separated from the breeder region by a water-cooled panel, the water-cooled $LiAlO_2$ breeder region, and a graphite reflector. First-wall blanket design parameters are summarized in table 9.

3.3.2.1. First-wall and blanket structure. The water-cooled austenitic stainless steel first wall is a panel

Table 9
Summary of blanket design parameters

First-wall/blanket parameters	
Structural material	Advanced austenitic stainless steel
Structural wall thickness (mm)	1.5
Maximum structural temperature (°C)	<450
Coating/cladding	Beryllium
Coating/cladding thickness (mm)	1.0
Coolant	Pressurized water
Coolant outlet temperature (°C)	320
Coolant inlet temperature (°C)	280
Coolant velocity (m/s)	10
Breeding region	
Structural material	Advanced austenitic stainless steel
Maximum structural temperature (°C)	425
Breeder material	α-$LiAlO_2$
Theoretical density (g/cm^3)	3.4
Effective density (%)	60
Grain size (10^{-6} m)	0.1
Maximum temperature (°C)	850
Region thickness (m)	0.4
Coolant	Pressurized water
Coolant inlet temperature (°C)	280
Coolant outlet temperature (°C)	320
Neutron multiplier	
Material	Zr_5Pb_3
Maximum temperature (°C)	900
Thickness (m)	0.07
Density (g/cm^3)	8.9
Reflector	
Material	Graphite
Thickness (m)	0.15
Maximum temperature (°C)	<900
Structure	Low molybdenum stainless steel
Structure temperature	<450°C

coil-type construction and is an integral part of the blanket module. The coolant temperature is maintained between 280 and 320°C throughout the first-wall and blanket. For the average neutron wall loading of 3.6 MW/m^2 the average surface heat flux on the first wall is 0.92 MW/m^2 with a peak-to-average value of ~1.2. The maximum structural temperature in a 1.5-mm thick stainless steel wall is 450°C for the reference conditions. For these low temperatures, an estimated wall design life of ~20 MW/m^2 is considered reasonable for an advanced austenitic stainless steel.

The proposed panel coil-type construction provides integral cooling of the blanket wall and avoids the necessity for a large number of tube welds in the high radiation zone. Since fabrication by a roll-bonding process does not greatly affect the microstructure of the steel, radiation damage in the weld region should not differ substantially from the bulk material. Also, the panel coil structure is perceived to have less vibration problems than an unsupported tube bank.

A ~1-mm thick beryllium coating or clad on the first wall serves to protect the plasma from the high-Z wall material. This thickness will provide sufficient material to withstand the surface erosion for the blanket lifetime of ~6 yr. A slightly thicker beryllium coating may be required on the inboard wall to accommodate the projected number (~10 per wall lifetime) of plasma disruptions.

3.3.2.2. Tritium breeding zone. The ~40-cm tritium-breeding zone consists of a packed bed of α-$LiAlO_2$ with 1-cm diameter stainless steel coolant tubes

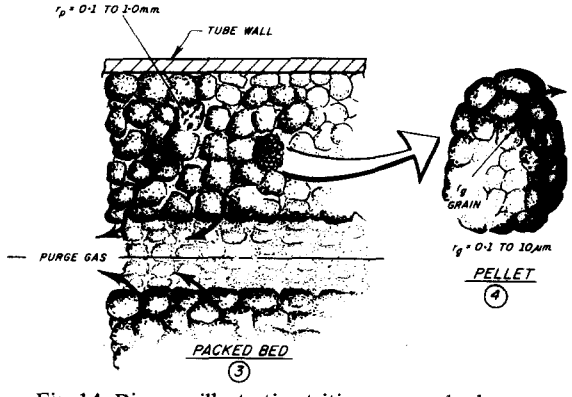

Fig. 14. Diagram illustrating tritium removal scheme.

spaced appropriately throughout the zone to maintain a maximum breeder temperature of 850°C. The tube spacing increases from ~2 cm at the front of the breeder zone to 5–10 cm at the back. The coolant inlet temperature is 280°C with an outlet temperature of 320°C. The relatively low temperature of the austenitic stainless steel tubes (<400°C) and the oxide film on the water side of the tubes provide an adequate tritium barrier for inleakage into the coolant. The $LiAlO_2$ is perforated with ~2 mm diameter holes through which low-pressure (~1 atm) helium passes to recover the tritium from the breeder. The $LiAlO_2$ is ~60% dense to facilitate percolation of tritium (as T_2O) to the helium purge channels. Fig. 14 is a schematic diagram that illustrates the tritium removal scheme. Tritium generated within $LiAlO_2$ grains diffuses to the surface of the grains, desorbs from the grain surface as T_2O, migrates along interconnected grain boundary porosity to the surfaces of the breeder particles, and finally percolates through the particle bed to the helium purge channels where it is carried to the processor.

Maximum lithium burnup in the blanket region will be ~25% for a first-wall lifetime of 20 MW-y/m^2. In addition to changing the stoichiometry of the breeder material, breeding characteristics and the energy generation profile in the blanket will be affected. When a neutron multiplier is used, the tritium breeding comes almost exclusively from ^{6}Li. Therefore, highly enriched lithium (>50% ^{6}Li) is used to minimize the lithium and tritium inventories. Although some tradeoffs are possible, a limit of ~20 MW-y/m^2 is reasonable for the breeder. This restriction tends to limit the value of a longer lifetime structure for a solid breeder blanket.

3.3.2.3. Neutron multiplier. The proposed Zr_5Pb_3 neutron multiplier provides some of the benefits of a lead multiplier while maintaining the design simplicity of the solid state materials. These advantages include a more uniform burnup and energy generation rate in the blanket region. The maximum lithium burnup in the blanket region is ~50% higher with a beryllium multiplier. Burnup of the multiplier is also reduced with the heavier elements (zirconium and lead) since the n, 2n reaction simply leads to the formation of another isotope of the same element in most cases. A multiplier zone thickness of ~7 cm is

required to provide sufficient multiplication. The back side of the first wall and a water-cooled panel between the multiplier and breeder zones provides cooling for the 7-cm slab. Approximately 30% of the neutron heating is deposited in the multiplier zone with maximum temperatures of the Zr_5Pb_3 calculated to be ~900°C. Additional blanket structure will be required to support the ~5×10^5 kg (500 tons) of neutron multiplier.

3.3.2.4. Reflector, manifold, and structural support. The reflector consists primarily of ~15 cm of graphite. The 20-cm support structure to which the blanket modules are attached also serves as the containment for the graphite reflector. In order to conserve space, the manifolding for the blanket is imbedded in the graphite reflector. The manifolding with appropriate additional channels serves as the coolant for the reflector region. A modified austenitic steel with low molybdenum content is used in this low-flux region to reduce the long-term activation.

3.3.2.5. Total module. The total blanket module, with a thickness of 68 cm, consists of a 1-cm thick first wall, a 7-cm thick neutron multiplier, a 40-cm thick breeding zone, and a 20-cm thick reflector that contains the blanket support structure and the manifolding. The modules are 2–3 m wide by ~3 m high depending on the location within the reactor. The module walls and all support structures in the high-radiation zone are fabricated from an advanced low-swelling austenitic stainless steel. All internal structure is integrally cooled to remove the nuclear heating and maintain the structure below 400°C.

For plasma stability, an electrical conducting path equivalent to 2 cm of stainless steel is required near the first wall. The conductivity of the first wall and the neutron multiplier meets this requirement in the modules. Between modules, a conducting path in the wall of the module to the back of the blanket and across a jumper to the next module is provided to complete the electrical circuit.

3.3.3. Power conversion system

The power conversion system, shown schematically in fig. 15, is utilized to convert the reactor thermal energy to electrical power. Two separate heat removal circuits are utilized, one for the first wall/blanket and the other for the limiter. The power deposited in the limiter (200 MW) is used for feedwater heating while the recoverable power (3800 MW) from the first wall and blanket is used to produce steam at 299°C and 6.3 MPa. The steam is then used in a turbine-generator unit for producing

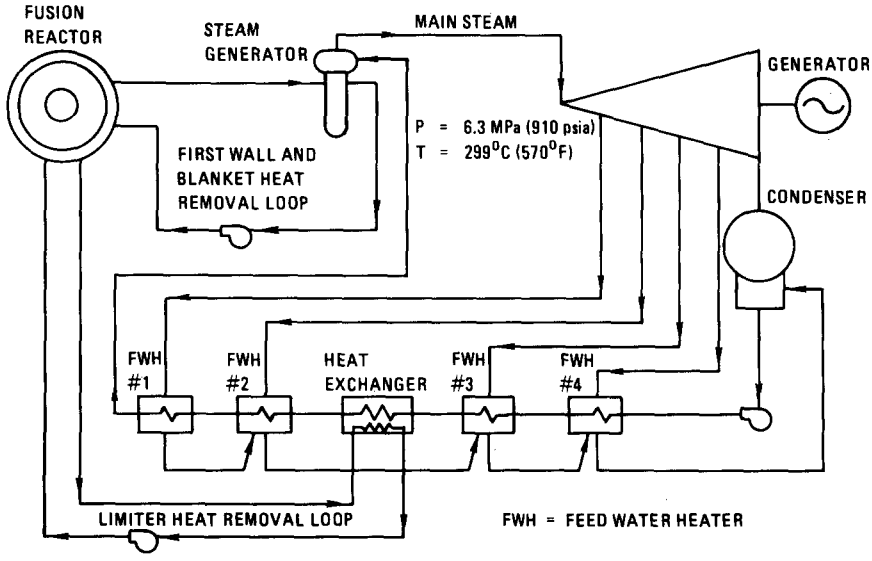

Fig. 15. Power conversion system schematic.

1440 MW of electrical power. The net electrical power is 1200 MW with 240 MW recirculating power for the rf system, coolant pumps, and other reactor subsystems.

3.4. Radiation shielding

The functions of the shielding system are: (1) to protect reactor components from radiation damage and nuclear heating, as well as reduce induced activation that may result in maintainability and disposal problems; and (2) to protect workers as well as the general public from radiation exposure at all times during operation, shutdown, scheduled maintenance, and unscheduled failures. The shield system in STARFIRE consists of the blanket, primary bulk shield, penetration shield, component shield, and biological shield.

The interrelations among the shield and reactor components in a fusion reactor are strong and complex. The shield design in STARFIRE has evolved from a comprehensive approach that involved the following: (1) recognition of the importance of the shield system and its impact on reactor component reliability, simplicity, maintainability, and economics; (2) full account of the shielding considerations in the selection process of key reactor subsystems from the early stages of the reactor design – clear examples of this are the choice of the limiter instead of divertor for plasma impurity control and exhaust and the selection of lower hybrid rf system for plasma auxiliary heating in preference to neutral beams; and (3) comprehensive tradeoff analyses for determining the material composition and dimensions of the shield components. The key features of the bulk and penetration shields are summarized in the rest of this subsection.

3.4.1. Bulk shield

The primary bulk shield circumscribes the blanket and consists of two parts: (1) the inboard shield; and (2) the outboard shield. The distinction between the inboard and outboard shields is necessary as the design objectives and constraints are quite different in the two regions.

The main function of the inboard shield is to protect the components of the superconducting TF coils. The overriding design constraint on the inboard shield is the large sensitivity of the reactor performance and economics to the radial thickness, Δ^{i}_{BS}, from the first wall to the location of the maximum magnetic field. In order to minimize Δ^{i}_{BS}, shielding materials with large radiation attenuation efficiency are used. The value of Δ^{i}_{BS} is 1.2 m. This includes space for 7-cm vacuum gaps between the blanket and shield, shield and TF coils, and thermal insulation inside the TF vacuum tank; 3-cm vacuum tank (stainless steel); and 7-cm helium vessel (stainless steel). The inner blanket is 34 cm thick and must breed tritium as the tritium breeding margin with solid breeders is small. Thus, the space available for the inboard bulk shield is 67 cm. This consists of 12 cm water, 7 cm 304 stainless steel, 7 cm lead, 18 cm boron carbide, and 23 cm tungsten. The use of expensive materials (tungsten and boron carbide) is justified because the volume of the inboard shield (being on the inner side of the torus) is relatively small and the additional expense is more than compensated for by the reduction in reactor size when Δ^{i}_{BS} is reduced due to the increase radiation attenuation obtainable with tungsten and boron carbide.

The maximum dose in the TF coil insulators after 30 yr of irradiation is $\sim 5 \times 10^{9}$ rad. Some organic insulators such as kapton have been shown [19] recently to withstand a radiation dose of $\sim 10^{10}$ rad at cryogenic temperatures. The maximum radiation-induced resistivity in the copper stabilizer is $\sim 5 \times 10^{-10}$ Ωm after irradiation corresponding to an integral neutron wall load of 20 MW-yr/m^2. This is the expected lifetime of the first-wall/blanket structure. In addition, the reactor plant maintenance plans call for ~4-mo shutdown every ~5 yr. Magnet anneal will be conveniently made every ~5–7 yr in parallel to other maintenance tasks. The maximum change in the critical current density of the superconductor is ~2% after 20 MW-yr/m^2 irradiation. It should be noted that radiation effects in the magnet components are greatly reduced with depth as a result of strong radiation attenuation within the magnet. In addition, the magnetoresistivity decreases and the critical current density increases with depth within the magnet. Therefore, the TF coil cross section has been designed with several spatial grades to minimize the amount of stabilizer and superconductor.

One of the functions of the outboard shield is similar to that of the inboard shield; namely radiation

protection of TF coils. The space at the top, bottom, and outer side of the reactor is not as restrictive as that on the inside. However, because of its geometrical location and relatively large volume, the outboard shield must satisfy an additional number of design requirements. Since the volume of materials in the outboard shield is rather large (~1000 m^3), shielding materials with no or low long-lived radioactivity should be selected to minimize the need for long-term radwaste storage and to permit recycling. Furthermore, the outboard shield should provide neutron attenuation sufficient to prevent significant production of long-lived isotopes in the large volumes of materials in the TF and external EF coils and other reactor components outside the bulk shield. Another important requirement is that the reactor building concrete wall should not be significantly activated nor should it require forced cooling. All of these design requirements on the outboard shield should, of course, be simultaneously applied to the penetration shield as discussed shortly.

An extensive scoping study for the outboard shield resulted in defining three combinations of shielding materials for the final design selection. These are: (1) 45% 304 stainless steel plus 45% B_4C plus 10% light water (H_2O); (2) 20% type 4381 titanium alloy (Ti 4381) plus 20% lead plus 30% B_4C plus 30% H_2O; and (3) 20% type 2024 aluminum alloy (Al 2024) plus 20% lead plus 30% B_4C plus 30% H_2O. Any of these combinations would be 0.8-m thick followed by 0.1-m thick region of 90% lead plus 10% B_4C. All percentages here are on a per volume basis.

Fig. 16 shows the biological dose rate at one day after shutdown in the reactor hall outside the bulk shield for the three shielding compositions. All three compositions are capable of reducing the dose rate to ~2.5 mrem/hr which is the current regulatory limit for occupational exposure based on 40 hr/wk and 50 wk/yr work load per person. Although the STARFIRE plans call for fully remote maintenance, the results in fig. 16 show that personnel access into the reactor hall with all shielding in place is permissible within one day after shutdown. This provides a degree of confidence in improving the plant availability factor, if desired, by permitting some maintenance task to be carried out in contact or semi-remote mode.

Fig. 17 shows the total radioactivity level in the outboard bulk shield for the three candidate compositions as a function of time after shutdown. The results are

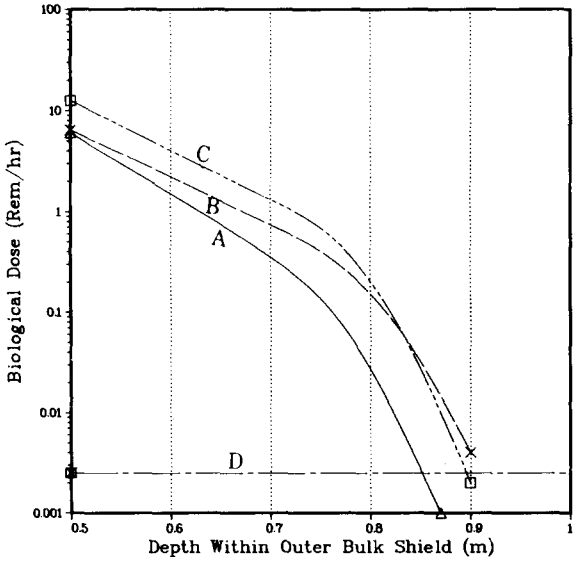

Fig. 16. Impact of shield material selection on biological dose after reactor shutdown. Case A: 45% SS-304 + 45% B_4C + 10% H_2O; Case B: 20% Al-2024 + 20% Pb + 30% B_4C + 30% H_2O; Case C: 20% Ti-4381 + 20% Pb + 30% H_2O; and Case D: NRC limit. (Neutron wall load = 3.6 MW/m^2, reactor operation = 5 yr; and time after shutdown = 1 day.)

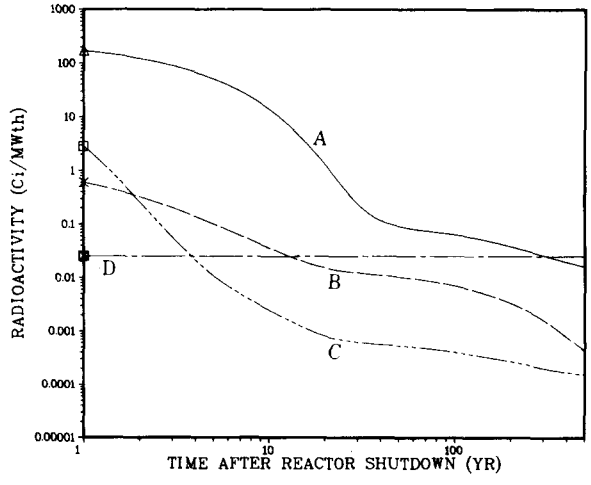

Fig. 17. Impact of shield material selection on induced radioactivity in outer bulk shield. Case A: 45% SS-304 + 45% B_4C + 10% H_2O; Case B: 20% AL-2024 + 20% Pb + 30% B_4C + 30% H_2O; Case C: 20% Ti-4381 + 20% Pb + 30% B_4C + 30% H_2O; and Case D: low level waste (LLW) limit. (Neutron wall load = 3.6 MW/m^2; and reactor operator = 5 yr.)

normalized to curies per megawatt of plant thermal power. A specific radioactivity level below 10^{-7} Ci/m^3 is normally classified as low-level waste (LLW) for which no special shield is required. Material recycling of LLW into future reactors may be economically and environmentally feasible. The average specific radioactivity decays into the low-level range in ~5 yr for the titanium system (composition No. 3 defined above) compared to ~15 and 300 yr for the aluminum (composition No. 2 defined above) and stainless steel (composition No. 1 defined above), respectively.

The shield composition of 20% titanium + 20% lead + 30% B_4C and 30% H_2O has been selected for the reference design as it offers distinct environmental advantages. Replacing the titanium with aluminum is slightly less desirable, but is considered an acceptable alternative.

3.4.2. Penetration shielding

One of the important design considerations is the radiation streaming through the void regions that penetrate the blanket and bulk shield system. In the STARFIRE design study, a serious effort has been devoted to minimizing the number and size of penetrations as well as to perform a detailed multi-dimensional neutronics analysis in order to ensure adequate radiation shielding. The most important penetrations with regard to the design are: (1) pumping ports in the bulk shield for torus evacuation; (2) the limiter slot opening leading to the vacuum plenum for plasma impurity control; and (3) rf waveguides for the plasma current drive and plasma heating system.

A particle transport analysis was carried out using the Monte-Carlo code, MORSE-CG, with 14 000 neutron histories. The analysis was done for the vacuum pumping ports and rf waveguides which were completely surrounded by a shield tentatively chosen to be 0.5-m thick 50% stainless steel plus 50% B_4C. The choice of the penetration shield material and its thickness has a significant impact on the radiation damage and induced activation of reactor components external to the penetrations. An extensive analysis on the shield optimization is now underway and the analysis in the present study will be reiterated as better shielding materials evolve from the optimization analysis.

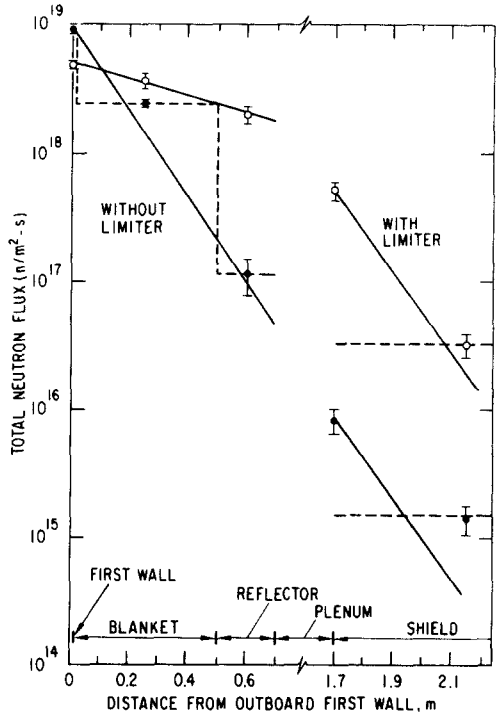

Fig. 18. The effect of the limiter slot opening on the radiation streaming. (Average neutron wall load = 3.6 MW/m^2; limiter opening height = 0.4 m; and number of neutron histories = 14 000.)

Nuclear heating due to radiation streaming into the cryopumps is of concern. The vacuum duct in the reference design is cylindrical with a 1-m diameter and penetrates through the bulk shield with a slope of 45 deg to the reactor centerline. It is found that the nuclear heating rates in copper and stainless steel cryopanels are approximately the same, and the lowest heat load occurs in aluminum cryopanels. None of the three materials examined is likely to pose any difficult cryogenic heat removal problem, provided that the duct length is longer than ~3 m (for which the heat loads are 0.5, 0.6, and 0.3 kW/m^3 in stainless steel, copper, and aluminum panels, respectively, with a typical error estimate of ~30%).

Fig. 18 shows the effect of the limiter slot opening upon the radiation enhancement in the outboard shield region. It is seen that the maximum and average neutron fluxes in the shield are increased by a factor of 60–20 due to the presence of the limiter slot (slot height of 0.4 m entirely in the toroidal

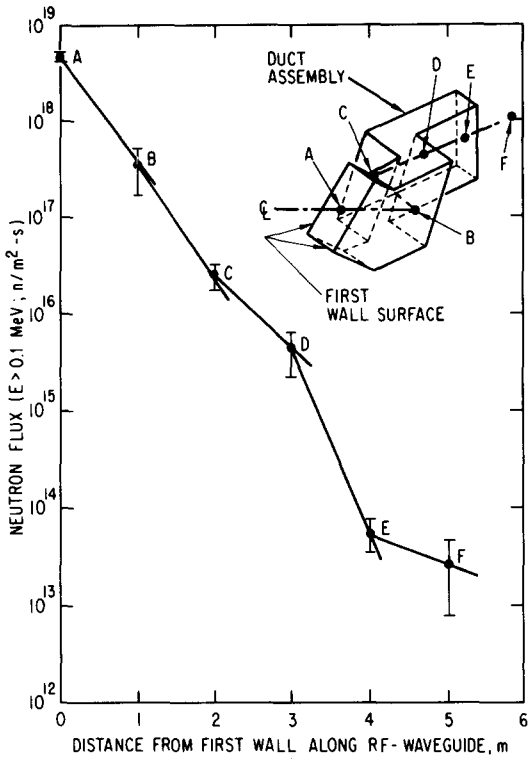

Fig. 19. The variation of neutron fluence along the rf waveguides. (Average neutron wall load = 3.6 MW/m^2; rf duct opening = 2.7 m X 0.43 m; and number of neutron histories = 14 000.)

direction on the reactor midplane) followed by a 1-m wide vacuum plenum gap. It is of importance to point out that the neutron flux at the vacuum pumping port entrance is ~1.4×10^{16} (±29%) n/m^2-s in the case with the limiter, compared to a flux of ~8.2×10^{15} (±22%) n/m^2-s in the case without limiter. The implication is that the radiation enhancement into the vacuum ports caused by the limiter opening is not excessive and the radiation streaming into the vacuum ports from particles penetrating through the blanket region adjacent to the ports is equally important.

Fig. 19 presents the neutron flux through an rf waveguide whose opening is rectangular (~27 m X 0.43) consisting of stainless steel grids of 12 rows X 9 grills (this is an earlier version of the rf design but the attenuation characteristic should not be largely different). Under the condition of two duct bends, none of the candidate dielectric window materials located behind the plenum region appears to be exposed to a neutron fluence of more than 10^{25} n/m^2 over a 10-yr operation at a neutron wall load of 3.6 MW/m^2. It is important to note that even without the 90-deg bends behind the reflector, an Al_2O_3 ceramic window is likely to be durable over the same operation time as long as it is placed behind the bulk shield.

3.5. Magnetic systems

3.5.1. Toroidal field system

The 12-element TF coil system for STARFIRE is required to generate 5.8 Tesla at the 7.0-m plasma axis with a maximum field ripple of ±1.5%. Coil bore spatial conditions dictate a 3.0-m mean centerpost radius and a 13.0-m mean outer leg radius, with a peak field requirement of 11 Tesla (2.0×10^8 A-turns).

Nb_3Sn has been selected for the superconductor material in the high field region, based upon anticipated lower costs of production by the end of the century. Niobium-titanium alloy, operating at a bath temperature of 3 K is considered an acceptable alternative. Helium bath cooling has been selected over forced-flow concepts on the basis of design simplicity and operational reliability.

Selection of a flat 24-kA cabled conductor geometry has the following advantages over the monolithic designs: high-cooled surface-to-volume ratio; conventional modular construction (strand, subcable, cable) yielding large composite strand area reduction (and hence peak performance); minimum a–c loss characteristics; and, for Nb_3Sn, the capability for reaction before winding without the imposition of severe post-cure handling restrictions. In the selected design, the conductor is supported against hoop tensile and transverse bearing loads by an enclosing 'box' of prestressed stainless steel support strips.

The STARFIRE TF coils are supported against the overturning forces due to the external poloidal field coils. Support of such loads (15×10^6 lb/coil) requires heavy cryostat walls, and a large total cross-sectional area of cold-to-warm helium vessel supports which results in ~400 W of conductive heat leakage.

The common inner dewar of the TF coils should have a long L/R time to protect the TF coils from excessive eddy-current heating resulting from a

plasma disruption. On the other hand, it should have a short L/R time in order that the copper EF coils near the dewar will not be made ineffective by image currents in the dewar. This conflict is resolved by using stainless steel as the dewar material, making it thicker (3 cm) near the midplane, where plasma disruption effects on the TF coils are important, and making it thinner (1 cm) near the copper EF coils.

3.5.2. Poloidal field coil systems

The EF coil system for a tokamak reactor has several important functions in addition to its fundamental role of balancing the plasma hoop expansion force. It provides the fields that generate plasma elongation and provides stability of the equilibrium to axisymmetric modes, interchange modes, and ballooning modes.

Vertical positional control is another important function of the EF coil system. Plasmas with vertical elongation tend to be inherently unstable to vertical displacements. Similarly, changes in the plasma pressure or current density profile can result in radial drifts of the plasma position. These drifts or displacements, if uncorrected by currents in the EF coil system, can result in plasma disruptions through interaction of the plasma with the vacuum chamber wall.

In the STARFIRE design, it was decided that the main EF coils should be superconducting and should all lie outside the toroidal field coils, in order to facilitate repair or replacement of the poloidal or toroidal coils. Although an outside coil system increases the stored energy and total current in the assembly, maintainability and reliability of the EF coils should be far superior to an inside EF coil system. With outside coils, however, it is important to minimize the toroidal field coil size, since the required EF coil currents increase exponentially with distance from the plasma [20].

A small OH system supplying 25 V-s is provided for STARFIRE to bring the plasma current to the level of 1–2 MA where the rf current drive can take over. This system, shown in fig. 3, consists of six coils, symmetric about the midplane. More volt-seconds could be provided by putting additional coils in the inboard region. The OH system was designed to have zero field everywhere in the plasma to within about 0.4% of the peak EF field.

The external field necessary to keep the plasma in equilibrium can be calculated for the STARFIRE reference MHD equilibrium described in section 3.1. The EF coil currents, for given locations, are determined by making a least-squares fit to the calculated field, simultaneously minimizing the stored energy and decoupling the EF coils from the OH coils. The method is described in detail in ref. [20]. The locations are then chosen to make the best EF system consistent with the structure of the device. Since the OH and EF systems must be driven independently, the decoupling insures that a current change in either system will not induce voltages in the other.

The EF coil system chosen for STARFIRE consists of eight coils, symmetric about the midplane (see fig. 3). At peak plasma current, the total current in the EF system is 86 MA with a stored energy of 10 GJ. The EF system provides 80 V-s to the plasma in addition to the OH system volt-seconds.

In STARFIRE the plasma current startup period will be of the order of 1 min. The power supply for the EF coils will be supplied by power directly from the utility power grid; no electrical energy storage will be required. Rapid or sudden changes in the plasma position, due for example to modifications of the current profile by MHD activity or to vertical instability, cannot be followed by the external EF coil system without oversizing of the power supplies and without difficult constraints on coil manufacture due to the high voltage to be applied to the terminals. It is more practical to place demountable copper coils as near to the plasma as possible for the purpose of plasma control. The STARFIRE design has four copper control coils located outside the blanket and shield which are feedback controlled and carry little average current. (See fig. 3.) The common TF coil dewar is thinned locally to reduce the L/R time-of-image currents to <20 ms, so effective control is possible.

Modeling of the equilibrium shows that currents up to 0.5 MA may be required in the control coils to stabilize vertical displacements of 20 cm, which is the plasma scrape-off layer thickness. The power required from the feedback amplifier can be determined when the time scale for plasma motions is known. In the absence of a conducting shell, the vertical displacement grows with a time scale of about 10 μs, given by the minor radius divided by the poloidal Alven speed. The control coils could not respond on this time scale

with a manageable level of power. If, however, the first walls of the blanket sectors are connected in the toroidal direction by intersegment jumpers at the rear of the blanket, the time scale will increase to the L/R time, about 40 ms. The peak reactive power for the control coils is then about 500 MW, while the resistive power can be kept below 5 MW. The resistance of the conducting shell is sufficient that the ohmic heating voltage does not drive more than 20 kA in the first wall.

The conducting shell also plays an important role in the stabilization of the low-mode number kink instability. Analysis of the plasma using the computer code ERATO shows that these kinks are unstable, but that a conducting wall within 20 cm of the plasma surface acts to stabilize the $n = 0$ and $n = 1$ modes. Higher mode numbers have reduced growth rates, but may require a closer wall for complete stabilization.

4. Reactor maintenance concept

The maintenance concept is based on the premise that STARFIRE is the tenth commercial power plant and that sufficient research and development has been performed and enough operating experience has been gained to have resulted in a predictable reactor. As a result, the design uses a 'remove and replace' approach that minimizes the number of replaceable assemblies and the number of required different maintenance operations. This approach increases confidence in the speed of maintenance operations and simplifies maintenance equipment design requirements.

Remote maintenance is planned for all reactor maintenance operations to minimize radiation exposure to maintenance personnel and because the reactor hall will be exposed to some tritium and decay radiation during maintenance operations. Use of remote equipment can also permit sone repairs while the reactor is operating.

All components within the reactor building are replaceable. Some are replaced on a scheduled maintenance basis while others are designed for the life of the plant and are replaced only in the event of failure. Items designed for the life of the plant include the overhead crane, TF coils, EF coils, coolant piping, reactor support structure, and shield. The blanket sector assemblies including limiters, rf ducts and fueling assemblies, shield door seals, vacuum pump isolation valves, etc., are replaced on a scheduled basis.

Redundancy is planned for some reactor auxiliary subsystems to permit continued operation of the plant until a scheduled maintenance period is reached or until the component can be replaced in-service.

Spares are provided for all components with potentially high failure rates, so that as one part is removed, a pretested replacement is installed so reactor operation can continue while damaged or end-of-life assemblies are moved from the reactor to a hot cell where more time and equipment are available for checkout, repair, or disposal.

The spares for the superconducting EF coils trapped below the TF coils are stored in place so reactor disassembly is unnecessary in event of a failure. These coils are designed for the life of the plant but the consequence of their failure suggests in-place spares are prudent. Spares are also provided for the large outer EF coils so that the reactor hall door size can be limited to that required for the TF coil.

Availability goals have been established as 85% for the reactor and 75% for the complete plant including the reactor. Allocations of permissible time-to-repair and time-between-failures have been made for major subsystems to serve as a basis for design of the components and maintenance equipment. These are shown in table 10. The mean-time-to-repair (MTTR) allocations are based on the average repair time for a typical failure. The average downtime per year is applicable only to those failures that result in a plant shutdown and do not include failures of components where redundant systems prevent an outage. The maintenance scenario incorporates the current utility practice of shutting down annually for one month of maintenance and a four-to-five month shutdown every five to ten years for turbine repair. The resultant permissible downtime goal per calendar year has been allocated as 39 days for scheduled maintenance of the entire plant and reactor and 21 days for unscheduled maintenance of the balance of plant. The 39 day shutdown includes a 9 day allowance for a 120 day shutdown every 10th year and a 30 day shutdown during the other 9 years. Scheduled reactor component replacement and repair is done on a non-interference basis in parallel with the balance-of-

Table 10
Unscheduled maintenance (forced outage)

Subsystem	MTTR [a] (days)	Average downtime per year (days)	Permissible failure rate per year [b]
Shield sector	90	2	0.04
rf system	6	0.6	0.1
Blanket system (including limiter)	30	10	0.2
Vacuum system	10	2	0.2
Fueling system	4	0.4	0.1
Magnet system – TF	350	4	0.012
Magnet system – EF	60	1	0.016
Primary coolant	10	2	0.2
Auxiliary coolant			
H_2O	10	2	0.2
GHe	10	2	0.2
LN_2	10	2	0.2
Power supplies	4	2	0.5
Maintenance equipment	2 [c]	1	0.5
Total		31	

[a] Mean-time-to-repair; includes startup and shutdown and fault isolation.
[b] For failures resulting in an outage.
[c] Occurs during outage only.

plant repair during the 30 day shutdown. Convenient preventive maintenance and repair of redundant components is included as part of the maintenance scenario during unscheduled outages.

A normal scheduled reactor maintenance interval would include four manipulators working on the reactor at 90-deg intervals. Blanket sectors would be replaced at two locations while vacuum pump isotation valves are replaced at the other two locations.

Acknowledgements

The authors are grateful to Ms. Cyrilla Hytry for her effort in compiling and typing this paper. This work was supported by the U.S. Department of Energy under Contract W-31-109-Eng-38.

References

[1] C.C. Baker, et al., STARFIRE, A commercial tokamak power plant design – Final report, Argonne National Laboratory, ANL/FPP-80-1 (1980).
[2] M.A. Abdou, D.A. Ehst and L.M. Waganer, Results of systems studies for the STARFIRE commercial tokamak, Proc. 8th Symp. on Engineering Problems of Fusion Research, San Francisco, 1979, to appear.
[3] D.J.H. Wort, Plasma Phys. 13 (1971) 34.
[4] N.J. Fisch, Phys. Rev. Lett. 41 (1978) 873; C.F.F. Karney and N.J. Fisch, Phys. Fluids 22 (1979) 1817.
[5] D.A. Ehst, Nucl. Fusion 19 (1979) 1369.
[6] D. Berger, L.C. Bernard, R. Gruber and F. Troyon, Plasma physics and controlled nuclear fusion research, Proc. 6th Intern. Conf. Berchtesgaden, 1976 (IAEA, Vienna, 1977) Vol. 2, p. 411.
[7] R.W. Moore, Report GA-A15353 (1979).
[8] M.P. Hacker and R.W. Harvey, Report GA-A14933 (1978).
[9] M. Brambilla, Nucl. Fusion 16 (1976) 47.
[10] S.Y. Yuen, J.H. Schultz, D. Kaplan and D. Cohn, Report RR-79-22, M.I.T. (1979).
[11] M. Gomolinski and G. Brebec, J. Nucl. Mater. 43 (1972) 59.
[12] Metals Handbook (American Society for Metals, Metals Park, Ohio 1979), 9th ed., Vol. 2.
[13] F.W. Wiffen, The tensile properties of fast reactor neutron irradiated BCC metals and alloys, Defects and Defect Clusters in BCC Metals and Their Alloys (Nuclear Metallurgy, 1973) Vol. 18, p. 176.
[14] J.M. Steichen, J. Nucl. Mater. 60 (1976) 13.
[15] Corrosion Data Survey on Tantalum (Fansteel Inc., Chicago, 1972).
[16] R. Jacobson, Princeton Plasma Physics Laboratory, private communication.
[17] R.W. Conn, I.N. Sviatoslavsky and D.K. Sze, Limiter pumping system for divertorless tokamaks, Proc. 8th

Symp. on Engineering Problems of Fusion Research, San Francisco, 1979, to appear.
[18] Y. Seki, V. Shimorua and K. Maki, Numerical calculations of helium ash enrichment and exhaust by a simple divertor, JAERI Memo 8605, Japan Atomic Energy Research Institute (1979).
[19] R.R. Coltman, Jr., C.E. Klabunde, R.H. Kernohan and C.J. Long, Effects of radiation at 5 K on organic insulators for superconducting magnets, Proc. 8th Symp. on Engineering Problems of Fusion Research, San Francisco, 1979, to appear.
[20] K. Evans, Jr., D.A. Ehst and P. Messerschmidt, Equilibrium-field coil considerations for tokamak reactors, ibid.